arXiv:1201.5430v2 [physics.comp-ph] 3 Oct 2012

Efficient FMM accelerated vortex methods in three dimensions via the Lamb-Helmholtz decomposition

Nail A. Gumerov* and Ramani Duraiswami†
Institute for Advanced Computer Studies
University of Maryland
College Park, MD 20742, USA

October 4, 2012

Abstract

Vortex methods are used to efficiently simulate incompressible flows using Lagrangian techniques. Use of the FMM (Fast Multipole Method) allows considerable speed up of both velocity evaluation and vorticity evolution terms in these methods. Both equations require field evaluation of constrained (divergence free) vector valued quantities (velocity, vorticity) and cross terms from these. These are usually evaluated by performing several FMM accelerated sums of scalar harmonic functions.

We present a formulation of vortex methods based on the Lamb-Helmholtz decomposition of the velocity in terms of two scalar potentials. In its original form, this decomposition is not invariant with respect to translation, violating a key requirement for the FMM. One of the key contributions of this paper is a theory for translation for this representation. The translation theory is developed by introducing "conversion" operators, which enable the representation to be restored in an arbitrary reference frame. Using this form, efficient vortex element computations can be made, which need evaluation of just two scalar harmonic FMM sums for evaluating the velocity and vorticity evolution terms. Details of the decomposition, translation and conversion formulae, and sample numerical results are presented.

1 Introduction

Vortex methods are used to simulate the Navier Stokes equation in the velocity–vorticity form with Lagrangian discretization. Since vortex particles are initially placed only in the region of finite vorticity and can convect along with the flow, these methods provide an optimized spatial discretization. Consider an incompressible flow generated by a set of N vortex elements, characterized by coordinates of the centers (sources) $\mathbf{x}_i$ and constant strength vector $\boldsymbol{\omega}_i$, $i = 1, ..., N$. Each element centered at location $\mathbf{x}_i$ produces an elementary velocity field $\mathbf{v}_i(\mathbf{y})$ according to the Biot-Savart law, and the total velocity field can be computed as a superposition of such elementary fields (e.g., see [2]):

$$\mathbf{v}(\mathbf{y}) = \sum_{i=1}^{N} \mathbf{v}_i(\mathbf{y}), \quad \mathbf{v}_i(\mathbf{y}) = \frac{\boldsymbol{\omega}_i \times (\mathbf{y} - \mathbf{x}_i)}{|\mathbf{y} - \mathbf{x}_i|^3} = \nabla \times \frac{\boldsymbol{\omega}_i}{|\mathbf{y} - \mathbf{x}_i|}. \tag{1}$$

In practice this field needs to evaluated at M evaluation points, $\mathbf{y}_j$, which has $O(MN)$ cost. The Biot-Savart kernel is composed of a vector of dipole solutions of the Laplace equation. It is well known that the Fast

*Corresponding Author. Also at Fantalgo, LLC., Elkridge, MD 21075; E-mail: gumerov@umiacs.umd.edu; Phone: +1-301-405-8210; Fax: +1-301-314-9658; web: http://www.umiacs.umd.edu/users/gumerov

†Also Department of Computer Science, and at Fantalgo, LLC. E-mail:ramani@umiacs.umd.edu, web: http://www.umiacs.umd.edu/users/ramani

Multipole Method (FMM) can be used to evaluate such sums to any specified accuracy ϵ at a $O(N+M)$ reduced cost [8].

The vortex elements move with the flow. This motion also causes an evolution of the vortex field according to the vortex evolution equation. For inviscid flow, the evolution equations for the vortex positions and strengths respectively are

$$\begin{aligned} \frac{d\mathbf{x}_i}{dt} &= \mathbf{v}|_{\mathbf{x}=\mathbf{x}_i}, \qquad \frac{d\boldsymbol{\omega}_i}{dt} = \mathbf{s}_i, \\ \mathbf{s}_i &= \boldsymbol{\omega}_i \cdot \nabla \mathbf{v}|_{\mathbf{x}=\mathbf{x}_i}, \quad \mathbf{v}\left(\mathbf{x}_i;t\right) = \sum_{j\neq i} \mathbf{v}_j\left(\mathbf{x}_i;t\right). \end{aligned} \tag{2}$$

Here the right hand side for the vortex strength is the so-called vortex stretching term, the evaluation of which requires the gradient of the velocity vector. The evolution equation for the vorticity can be modified to account for liquid viscosity. Also the elementary velocity field in Eq. (1) can be modified using a smoothing kernel, $K(|\mathbf{y}-\mathbf{x}_i|\,;a)$,

$$\mathbf{v}_i\left(\mathbf{y};a\right) = \frac{\boldsymbol{\omega}_i \times (\mathbf{y}-\mathbf{x}_i)}{|\mathbf{y}-\mathbf{x}_i|^3} K(|\mathbf{y}-\mathbf{x}_i|\,;a), \quad K(r;a) = 1 + O(\epsilon), \quad r \gg a, \tag{3}$$

which has an effect only on the near field, $r \lesssim a$, where a is the radius of the vortex core, which may change in time, and $\epsilon \ll 1$ is the tolerance for approximation. This modification does not affect the far field, which can also be computed with the tolerance $O\left(\epsilon\right)$ in an accelerated manner via the FMM. In the sequel we do not specify the core function $K(r;a)$; several choices including the Gaussian and polynomial forms are discussed in the literature (see e.g., [4, 19, 24, 25]), and there are several ways to speed up the local summation as well. Extensions to compressible flow are also possible [5].

The evolution equation is integrated using an appropriate time stepping scheme. The right hand side of this equation, also results in an N body computation for the influence of particles in the far-field, with somewhat more complicated terms. As discussed above, the FMM for the vortex element method is closely related to the scalar FMM for sums of multipoles of the Laplace equation ("harmonic FMM"). In fact, it is possible to start with a program for a harmonic FMM and appropriately modify it to create a fast vortex method. In terms of performance, computation of potential gradients and higher derivatives can be referred as "auxiliary" computations, which can be done as soon as local expansions for the potentials are available. In this sense the question as to how many independent potentials need to be computed to obtain right hand sides of the evolution equations (2) is important. For example, to compute the three components of the gravitational force in an stellar N-body computation one needs only one harmonic FMM; the gradients can be obtained via differentiation of expansions, which is done efficiently by application of sparse matrix operators to the potential expansions. Treating the problem in a straightforward way, for the vortex method, one should use three independent harmonic FMM sums (for each velocity component). However, because of the divergence constraint, one may speculate that it is possible to reduce this number to two. THat this in fact is so is a main result of the present paper.

A similar reduction of the complexity to solution of two harmonic FMMs was obtained for the biharmonic equation [13] (opposed to five FMMs using factorization [7]). For the Stokes equations, where the solution can be decomposed to the sum of Stokeslets and Stresslets, a representation via three harmonic potentials (Lamb-Helmholtz decomposition [20]) requires only three harmonic FMMs (see also [21]), while a more simple way based on factorization [22] shows that the evaluation can be done with a cost of four harmonic FMM calls.

In this paper we develop such an efficient version of the FMM for vortex methods, which achieves an evaluation of both the velocity and stretching term sums at a cost of only two scalar harmonic FMMs (this also can be reduced to one complex valued harmonic FMM since the physical fields are real). Our approach

is based on the Lamb-Helmholtz decomposition [20], which allows representation of the vector field in the form of two scalar potential fields. This form is however not invariant to translation, and cannot be used as is, with an FMM summation algorithm. We develop conversion operators that allow this form to be translated.

Section 2 of the paper introduces the problem and notation, and shows that the equations can be considered to be solutions of a *divergence constrained vector Laplace equation*. Section 3 develops the translation theory for such equations, which is the main mathematical result of the paper. Section 4 shows how the new translation theory can be used, together with a harmonic FMM, to create an FMM for vortex methods. Section 5 presents the results of numerical testing and some examples of FMM accelerated vortex element method computations. Section 6 concludes the paper. Mathematical details are provided in appendices.

2 Statement of the problem

We are given N vortex blobs of strength $\boldsymbol{\omega}_i$, $i = 1, ..., N$ located at points $\mathbf{x}_i$ and moving with the flow. The velocity field can be evaluated using either Eq. (1) or (3), which both have the same asymptotic far-field form. The evolution of the vortex positions and the vortex strengths is given by Eqs. (2). At $\mathbf{y} \neq \mathbf{x}_i$, $i = 1, ..., N$, the velocity field $\mathbf{v}(\mathbf{y})$ satisfies the divergence constrained vector Laplace equation (DCVLE)

$$\nabla^2 \mathbf{v} = \mathbf{0}, \quad \nabla \cdot \mathbf{v} = 0. \tag{4}$$

If the divergence of the field were not constrained, each Cartesian component of the velocity would be an independent harmonic function. The divergence constraint, however, reduces the degree of freedom for solutions by 1, and, in fact, only two harmonic scalar potentials, ϕ and χ, are necessary to describe the total field inside or outside a sphere centered at the origin

$$\mathbf{v}(\mathbf{r}) = \nabla\phi(\mathbf{r}) + \nabla \times (\mathbf{r}\chi(\mathbf{r})), \quad \nabla^2\phi = 0, \quad \nabla^2\chi = 0. \tag{5}$$

This decomposition can be treated as a general Helmholtz decomposition of an arbitrary vector field. Presumably, this form is due to Lamb [20], who used it to obtain a general solution for the Stokes equations in spherical coordinates, and we refer to this as the Lamb-Helmholtz decomposition. Indeed, Eq. (4) are the Stokes equations with zero pressure for which the Lamb solution provides (5).

The DCVLE appears naturally when one attempts to follow a general procedure to reconstruct an arbitrary vector field from given curl, $\boldsymbol{\omega}(\mathbf{r})$, and divergence, $q(\mathbf{r})$,

$$\nabla \times \mathbf{v} = \boldsymbol{\omega}, \quad \nabla \cdot \mathbf{v} = q. \tag{6}$$

The solution of these equations in free space can be written in the form (e.g. see [2]):

$$\mathbf{v}(\mathbf{y}) = -\nabla_{\mathbf{y}} \int_V \frac{q(\mathbf{x})}{4\pi |\mathbf{y} - \mathbf{x}|} dV(\mathbf{x}) + \nabla_{\mathbf{y}} \times \int_V \frac{\boldsymbol{\omega}(\mathbf{x})}{4\pi |\mathbf{y} - \mathbf{x}|} dV(\mathbf{x}). \tag{7}$$

Subdividing the space to the vicinity of evaluation point $\mathbf{y}$ (near field) and the domain outside this neighborhood (far field) and discretizing the integrals for the far field using quadratures with weights w_i and nodes $\mathbf{x}_i$, we obtain for the far field contribution

$$\begin{aligned} \mathbf{v}_f(\mathbf{y}) &= \sum_i \mathbf{v}_{fi}(\mathbf{y}), \quad \mathbf{v}_{fi}(\mathbf{y}) = -\nabla \frac{q_i}{|\mathbf{y} - \mathbf{x}_i|} + \nabla \times \frac{\boldsymbol{\omega}_i}{|\mathbf{y} - \mathbf{x}_i|}, \\ q_i &= \frac{w_i q(\mathbf{x}_i)}{4\pi}, \quad \boldsymbol{\omega}_i = \frac{w_i \boldsymbol{\omega}(\mathbf{x}_i)}{4\pi}. \end{aligned} \tag{8}$$

Hence, the far field satisfies Eq. (4) for which decomposition (5) can be used and just an addition to potential ϕ due to a given monopole distribution $q(\mathbf{x})$ provides solution for a general case. As mentioned,

in the present paper we do not address computation of the near field, which can be done locally, e.g. using appropriate smoothing kernels. Note that solution (7) of Eq. (6) is unique up to a gradient of a harmonic function Φ, which should be found from the boundary conditions. Such functions for a given boundary can be added to $\phi(\mathbf{r})$ in Eq. (5).

Equations (6) with $q \neq 0$ appear, e.g. in vortex methods for compressible flows. An example of equations (for 2D) can be found in [5], which can be appropriately modified for 3D. In terms of computational complexity, besides the velocity field and stretching term computations, also contraction of the velocity gradient tensor, $\beta = \nabla\mathbf{v} : \nabla\mathbf{v}$ should be computed in this case. This term can be computed simultaneously with computation of the vortex stretching term. Thus the cost in these extended cases should remain the same.

3 Translation theory for DCVLE

3.1 Basic translation and differential operators

Translation operator: A generic translation or shift operator $\mathcal{T}(\mathbf{t})$, where $\mathbf{t}$ is a constant termed the translation vector, acts on some scalar valued function $\phi(\mathbf{r})$, to produce a new function $\widehat{\phi}(\mathbf{r})$ (the translate), whose values coincide with $\phi(\mathbf{r})$ at shifted values of the argument

$$\widehat{\phi}(\mathbf{r}) = \mathcal{T}(\mathbf{t})[\phi(\mathbf{r})] = \mathcal{T}_{\mathbf{t}}\phi, \quad \widehat{\phi}(\mathbf{r}) = \phi(\mathbf{r}+\mathbf{t}), \quad \mathbf{r},\mathbf{t} \in \mathbb{R}^3. \tag{9}$$

This operator is linear. Also the translates of harmonic functions are also harmonic functions.

Elementary directional differential operators: We introduce the following notation for differential operators which appear in derivations:

$$\mathcal{D}_{\mathbf{r}} = \mathbf{r}\cdot\nabla, \quad \mathcal{D}_{\mathbf{t}} = \mathbf{t}\cdot\nabla, \quad \mathcal{D}_{\mathbf{r}\times\mathbf{t}} = (\mathbf{r}\times\mathbf{t})\cdot\nabla. \tag{10}$$

It can be shown that if $\phi(\mathbf{r})$ is a harmonic function in some domain, then $\mathcal{D}_{\mathbf{r}}\phi$, $\mathcal{D}_{\mathbf{t}}\phi$, and $\mathcal{D}_{\mathbf{r}\times\mathbf{t}}\phi$ are also harmonic functions in the same domain. Note also that operators $\mathcal{D}_{\mathbf{t}}$ and $\mathcal{D}_{\mathbf{r}\times\mathbf{t}}$ are related to an infinitesimal translation in the direction of vector $\mathbf{t}$ and an infinitesimal rotation about axis $\mathbf{t}$.

3.2 Conversion operators for the DCVLE

Consider the translation of the vector $\mathbf{v}(\mathbf{r})$ in (5). Using (9) for the translated functions,

$$\begin{aligned}\widehat{\mathbf{v}}(\mathbf{r}) &= \mathbf{v}(\mathbf{r}+\mathbf{t}) = \nabla\phi(\mathbf{r}+\mathbf{t}) + \nabla\times((\mathbf{r}+\mathbf{t})\,\chi(\mathbf{r}+\mathbf{t})) \\ &= \nabla\widehat{\phi}(\mathbf{r}) + \nabla\times((\mathbf{r}+\mathbf{t})\,\widehat{\chi}(\mathbf{r})) = \nabla\widehat{\phi}(\mathbf{r}) + \nabla\times(\mathbf{r}\widehat{\chi}(\mathbf{r})) + \nabla\times(\mathbf{t}\widehat{\chi}(\mathbf{r})).\end{aligned} \tag{11}$$

Obviously this is not form (5) representing $\widehat{\mathbf{v}}(\mathbf{r})$. Our goal is to find harmonic functions $\widetilde{\phi}$ and $\widetilde{\chi}$, which provide such a representation, i.e.

$$\widehat{\mathbf{v}}(\mathbf{r}) = \nabla\widetilde{\phi} + \nabla\times(\mathbf{r}\widetilde{\chi}). \tag{12}$$

For this purpose we introduce "conversion" operators $\mathcal{C}_{ij}$, $i,j = 1,2$:

$$\widetilde{\phi} = \mathcal{C}_{11}\widehat{\phi} + \mathcal{C}_{12}\widehat{\chi}, \quad \widetilde{\chi} = \mathcal{C}_{21}\widehat{\phi} + \mathcal{C}_{22}\widehat{\chi}, \tag{13}$$

which are linear due to the linearity of all transforms considered.

Comparing representations (11) and (12) we deduce, that $\widehat{\phi}(\mathbf{r})$ contributes only to $\widetilde{\phi}(\mathbf{r})$, leading to

$$\mathcal{C}_{11} = \mathcal{I}, \quad \mathcal{C}_{21} = 0, \tag{14}$$

where $\mathcal{I}$ is the identity operator. So, we can introduce harmonic functions ϕ' and χ' according to the following relations

$$\begin{aligned} \widetilde{\phi} &= \widehat{\phi} + \mathcal{C}_{12}\widehat{\chi} = \widehat{\phi} + \phi', \\ \widetilde{\chi} &= \mathcal{C}_{22}\widehat{\chi} = \widehat{\chi} + \chi'. \end{aligned} \tag{15}$$

Having two representations of $\widehat{\mathbf{v}}$, (11) and (12), and using Eq. (15), we obtain

$$\nabla\phi' + \nabla \times \left(\mathbf{r}\chi'\right) = \nabla \times \left(\mathbf{t}\widehat{\chi}\right). \tag{16}$$

Taking scalar product with $\mathbf{r}$ and noticing that $\mathbf{r} \cdot \nabla \times (\mathbf{r}\chi') = 0$, one can see that

$$\mathbf{r} \cdot \nabla\phi' = \mathbf{r} \cdot \nabla \times \left(\mathbf{t}\widehat{\chi}\right) = \mathbf{r} \cdot \left(\nabla\widehat{\chi} \times \mathbf{t}\right) = -\left(\mathbf{r} \times \mathbf{t}\right) \cdot \nabla\widehat{\chi}. \tag{17}$$

Another relation can be obtained if we take the curl of expression (16):

$$\nabla \times \nabla \times \left(\mathbf{r}\chi'\right) = \nabla \times \nabla \times \left(\mathbf{t}\widehat{\chi}\right). \tag{18}$$

It is not difficult to check that the following identities hold for the harmonic functions χ' and $\widehat{\chi}$:

$$\begin{aligned} \nabla \times \nabla \times \left(\mathbf{r}\chi'\right) &= \nabla\left(\chi' + \mathbf{r} \cdot \nabla\chi'\right), \\ \nabla \times \nabla \times \left(\mathbf{t}\widehat{\chi}\right) &= \nabla\left(\mathbf{t} \cdot \nabla\widehat{\chi}\right). \end{aligned} \tag{19}$$

Note that all scalar potentials are defined up to a constant. Therefore, we obtain from Eqs (18) and (19):

$$\chi' + \mathbf{r} \cdot \nabla\chi' = \mathbf{t} \cdot \nabla\widehat{\chi}. \tag{20}$$

Using (10) we can rewrite relations (17) and (20) in the form

$$\mathcal{D}_{\mathbf{r}}\phi' = -\mathcal{D}_{\mathbf{r}\times\mathbf{t}}\widehat{\chi}, \quad \left(\mathcal{I} + \mathcal{D}_{\mathbf{r}}\right)\chi' = \mathcal{D}_{\mathbf{t}}\widehat{\chi}. \tag{21}$$

In the next sections, we show that operators $\mathcal{D}_{\mathbf{r}}$ and $\left(\mathcal{I} + \mathcal{D}_{\mathbf{r}}\right)$ are invertible, and so we can write

$$\begin{aligned} \widetilde{\phi} &= \widehat{\phi} - \mathcal{D}_{\mathbf{r}}^{-1}\mathcal{D}_{\mathbf{r}\times\mathbf{t}}\widehat{\chi}, \\ \widetilde{\chi} &= \widehat{\chi} + \left(\mathcal{I} + \mathcal{D}_{\mathbf{r}}\right)^{-1}\mathcal{D}_{\mathbf{t}}\widehat{\chi}. \end{aligned} \tag{22}$$

Comparing Eqs (15) and (22), we obtain the following expressions for the conversion operators

$$\mathcal{C}_{12}\left(\mathbf{t}\right) = -\mathcal{D}_{\mathbf{r}}^{-1}\mathcal{D}_{\mathbf{r}\times\mathbf{t}}, \quad \mathcal{C}_{22}\left(\mathbf{t}\right) = \mathcal{I} + \left(\mathcal{I} + \mathcal{D}_{\mathbf{r}}\right)^{-1}\mathcal{D}_{\mathbf{t}}. \tag{23}$$

3.3 Expansions of harmonic functions

In addition to Cartesian coordinates we will use spherical coordinates (r, θ, φ):

$$\mathbf{r} = (x, y, z) = r\left(\sin\theta\cos\varphi, \sin\theta\sin\varphi, \cos\theta\right), \quad \mathbf{r} \in \mathbb{R}^3. \tag{24}$$

For expansions of the solutions of the Laplace equation that are regular inside or outside a sphere centered at the origin of the reference frame we introduce the regular or local functions $R_n^m\left(\mathbf{r}\right)$ and singular or multipole functions $S_n^m\left(\mathbf{r}\right)$, that are respectively defined as

$$\begin{aligned} R_n^m\left(\mathbf{r}\right) &= \frac{\left(-1\right)^n i^{|m|}}{(n+|m|)!} r^n P_n^{|m|}(\mu) e^{im\varphi}, \quad \mu = \cos\theta, \\ S_n^m\left(\mathbf{r}\right) &= \frac{i^{-|m|}(n-|m|)!}{r^{n+1}} P_n^{|m|}(\mu) e^{im\varphi}, \quad n = 0, 1, ..., \quad m = -n, ..., n, \end{aligned} \tag{25}$$

where $P_n^m(\mu)$ are the associated Legendre functions, defined by Rodrigues' formula

$$P_n^m(\mu) = \frac{(-1)^m \left(1-\mu^2\right)^{m/2}}{2^n n!} \frac{d^{m+n}}{d\mu^{m+n}} \left(\mu^2-1\right)^n, \; m \geqslant 0. \tag{26}$$

These functions are related to each other via

$$S_n^m(\mathbf{r}) = (-1)^{n+m}(n-m)!(n+m)! r^{-2n-1} R_n^m(\mathbf{r}). \tag{27}$$

The functions $R_n^m(\mathbf{r})$ and $S_n^m(\mathbf{r})$ defined above coincide with the normalized basis functions $I_n^m(\mathbf{r})$ and $O_n^m(\mathbf{r})$ considered in [6] and normalized spherical basis functions in [13]. The expansion of the Green's function in this basis is

$$|\mathbf{r}-\mathbf{r}_0|^{-1} = \sum_{n=0}^{\infty} \sum_{m=-n}^{n} R_n^{-m}(-\mathbf{r}_0) S_n^m(\mathbf{r}), \quad r > r_0. \tag{28}$$

Further, we represent harmonic functions in terms of sets of expansion coefficients over a certain basis centered at a given point, e.g. the local and multipole expansions centered at the origin are

$$\phi(\mathbf{r}) = \sum_{n=0}^{\infty} \sum_{m=-n}^{n} \phi_n^m F_n^m(\mathbf{r}), \quad \chi(\mathbf{r}) = \sum_{n=0}^{\infty} \sum_{m=-n}^{n} \chi_n^m F_n^m(\mathbf{r}), \quad F = R, S. \tag{29}$$

Absolute and uniform convergence of these series in the expansion regions is assumed below. We also extend the definition of the basis functions for arbitrary order m, to shorten some expressions

$$R_n^m(\mathbf{r}) = S_n^m(\mathbf{r}) = 0, \quad |m| > n, \quad n = 0, 1, ... \tag{30}$$

3.4 Matrix representation of operators

Let $\mathcal{L}$ be a linear operator, such that for harmonic function ϕ, $\psi = \mathcal{L}\phi$ is also a harmonic function. Assume further that both ϕ and ψ can be expanded into series of type (29). There should be a linear relation between the expansion coefficients $\mathbf{\Psi} = \{\psi_n^m\}$ and $\mathbf{\Phi} = \{\phi_n^m\}$, which, generally speaking, will have a form $\mathbf{\Psi} = \mathbf{L}\mathbf{\Phi}$, where $\mathbf{L}$ is a matrix, or representation of $\mathcal{L}$. Of course, for a given $\mathcal{L}$ the matrix $\mathbf{L}$ depends on the bases over which the expansion is taken.

Let $\phi(\mathbf{r})$ be expanded over basis $\{F_n^m(\mathbf{r})\}$, while $\psi(\mathbf{r})$ be expanded over basis $\{G_n^m(\mathbf{r})\}$. The action of the operator $\mathcal{L}$ on a basis function $F_n^m(\mathbf{r})$ can be represented as

$$\mathcal{L}F_n^m(\mathbf{r}) = \sum_{n'=0}^{\infty} \sum_{m'=-n'}^{n'} L_{n'n}^{m'm} G_{n'}^{m'}(\mathbf{r}), \quad n = 0, 1, ..., \quad m = -n, ..., n, \tag{31}$$

where $L_{n'n}^{m'm}$ are the reexpansion coefficients. It can be shown that the entries of matrix $\mathbf{L}$ are $L_{nn'}^{mm'}$, i.e. $\mathbf{L}$ is the matrix transpose of the matrix of reexpansion coefficients. Indeed,

$$\begin{aligned} \sum_{n=0}^{\infty} \sum_{m=-n}^{n} \psi_n^m G_n^m(\mathbf{r}) &= \psi(\mathbf{r}) = \mathcal{L}\phi(\mathbf{r}) = \sum_{n'=0}^{\infty} \sum_{m'=-n'}^{n'} \phi_{n'}^{m'} \mathcal{L}F_{n'}^{m'}(\mathbf{r}) \\ &= \sum_{n'=0}^{\infty} \sum_{m'=-n'}^{n'} \phi_{n'}^{m'} \sum_{n=0}^{\infty} \sum_{m=-n}^{n} L_{nn'}^{mm'} G_n^m(\mathbf{r}) = \sum_{n=0}^{\infty} \sum_{m=-n}^{n} \left[\sum_{n'=0}^{\infty} \sum_{m'=-n'}^{n'} L_{nn'}^{mm'} \phi_{n'}^{m'} \right] G_n^m(\mathbf{r}). \end{aligned} \tag{32}$$

The reexpansion coefficients for the translation operator $\mathcal{T}_{\mathbf{t}}$, Eq. (9), in the local and multipole bases (25) can be simply expressed via the respective basis functions (see [6] and [13]):

$$\begin{aligned} \mathcal{T}_{\mathbf{t}} F_n^m(\mathbf{r}) &= \sum_{n'=0}^{\infty} \sum_{m'=-n'}^{n'} (F|G)_{n'n}^{m'm}(\mathbf{t})\, G_{n'}^{m'}(\mathbf{r}), \quad F,G = S,R, \\ (R|R)_{n'n}^{m'm}(\mathbf{t}) &= R_{n-n'}^{m-m'}(\mathbf{t}), \quad (S|R)_{n'n}^{m'm}(\mathbf{t}) = S_{n+n'}^{m-m'}(\mathbf{t}), \quad (S|S)_{n'n}^{m'm}(\mathbf{t}) = R_{n'-n}^{m-m'}(\mathbf{t}). \end{aligned} \tag{33}$$

Here $(R|R)_{n'n}^{m'm}$, $(S|R)_{n'n}^{m'm}$, and $(S|S)_{n'n}^{m'm}$ are the entries of the local-to-local (L2L), multipole-to-local (M2L), and multipole-to-multipole (M2M) translation matrices, respectively. To obtain representations of other operators appeared above, we use differential relations for the basis functions, which also can be found in [6] and [13]:

$$\begin{aligned} \mathcal{D}_z R_n^m(\mathbf{r}) &= -R_{n-1}^m(\mathbf{r}), \quad \mathcal{D}_z S_n^m(\mathbf{r}) = -S_{n+1}^m(\mathbf{r}), \\ \mathcal{D}_{x+iy} R_n^m(\mathbf{r}) &= iR_{n-1}^{m+1}(\mathbf{r}), \quad \mathcal{D}_{x+iy} S_n^m(\mathbf{r}) = iS_{n+1}^{m+1}(\mathbf{r}), \\ \mathcal{D}_{x-iy} R_n^m(\mathbf{r}) &= iR_{n-1}^{m-1}(\mathbf{r}), \quad \mathcal{D}_{x-iy} S_n^m(\mathbf{r}) = iS_{n+1}^{m-1}(\mathbf{r}). \end{aligned} \tag{34}$$

where

$$\mathcal{D}_{x\pm iy} = \frac{\partial}{\partial x} \pm i\frac{\partial}{\partial y}, \quad \mathcal{D}_z = \frac{\partial}{\partial z}. \tag{35}$$

Appendix A provides explicit matrix representation of operators (10) and (23) required for numerical implementation of the present method.

4 Fast multipole method

There is an extensive literature on the FMM for the 3D Laplace equation (see, e.g., [8, 3, 9, 12, 15]), and we just present the modifications necessary to use this harmonic FMM for vortex methods.

Note that the FMM can be considered as a way to perform a dense matrix-vector product based on decomposition of the matrix into sparse and dense parts

$$\begin{aligned} \mathbf{v}(\mathbf{y}_j) &= \sum_{i=1}^{N} \mathbf{A}(\mathbf{y}_j, \mathbf{x}_i)\boldsymbol{\omega}_i = \sum_{\mathbf{x}_i \in \Omega(\mathbf{y}_j)} \mathbf{A}(\mathbf{y}_j, \mathbf{x}_i)\boldsymbol{\omega}_i + \sum_{\mathbf{x}_i \notin \Omega(\mathbf{y}_j)} \mathbf{A}(\mathbf{y}_j, \mathbf{x}_i)\boldsymbol{\omega}_i \\ &= \sum_{i=1}^{N} \mathbf{A}^{(sparse)}(\mathbf{y}_j, \mathbf{x}_i)\boldsymbol{\omega}_i + \sum_{i=1}^{N} \mathbf{A}^{(dense)}(\mathbf{y}_j, \mathbf{x}_i)\boldsymbol{\omega}_i, \quad j = 1, ..., M, \end{aligned} \tag{36}$$

where $\mathbf{x}_1, ..., \mathbf{x}_N$ are the sources, $\mathbf{y}_1, ..., \mathbf{y}_M$ are the receivers, $\Omega(\mathbf{y}_j)$ is a neighborhood of a box containing $\mathbf{y}_j$ which determines the sparse and dense parts of the matrix $\mathbf{A}$. Local summation, or sparse matrix-vector multiplication, is performed directly, while the dense matrix-vector product is found via generation of multipole expansions, translations, and evaluations of the local expansions. The present paper is about an efficient way to perform the dense matrix-vector product and does not consider acceleration of the sparse matrix-vector multiplication.

4.1 Complexity of the FMM

The relative cost of the different steps of the FMM depends on the source and receiver distributions, truncation number p, and the depth of the octree, $l_{\max}$, which hierarchically partitions the computational domain

Table 1: Comparison of the FMMs for the Laplace equation and for the VEM

FMM for Laplace equation	FMM for VEM	Comments
FMM set		
Create data structure	The same	octree, neighbor lists, etc.
Precompute translations	The same	only for a single potential
FMM run		
Create multipole expansions	Modified for two potentials	see Sec. 4.3
M2M translations	Modified for two potentials	Sec. 4.4
M2L translations	Modified for two potentials	Sec. 4.4
L2L translations	Modified for two potentials	Sec. 4.4
Evaluate expansions	Modified for two potentials	Sec. 4.5
Local summation	Add velocity and stretching	direct evaluation of partial sums (1) & (2)

occupied by N sources and M receivers. Simple cost estimates for the dense and sparse matrix-vector products can be provided for random uniform distributions and $M \sim N$:

$$C^{(dense)} = N\left(A_1 + \frac{A_2}{s}\right), \quad C^{(sparse)} = B_1 N s, \quad s = N \cdot 8^{-l_{\max}}, \tag{37}$$

where A_1 is the sum of costs of generation and evaluation of single expansions, constant A_2 is determined by the cost of translations per box, B_1 is the constant determined by the complexity of direct local summation for a single receiver, and s is the number of sources at level $l_{\max}$, which should be found from optimization. Note that qualitatively different $C^{(sparse)}$ dependence on N and s holds for some computing architectures, e.g. for graphics processors (GPUs) [15]. It is also noticeable that cost NA_1 can be neglected compared to other costs almost in all cases (and for simplicity we neglect it as well). In any case, theoretically, the optimum performance for a serial CPU implementation of the FMM can be achieved when the sum of the costs as a function of s reaches minimum, i.e.

$$s_{opt} = \sqrt{\frac{A_2}{B_1}}, \quad C_{opt}^{(dense)} \approx C_{opt}^{(sparse)} = N\sqrt{A_2 B_1}, \quad C_{opt}^{(total)} \approx 2N\sqrt{A_2 B_1}. \tag{38}$$

Based on this we can find theoretical complexity ratios of different versions of the FMM. As a reference we use a harmonic FMM for a single potential, where the gradient of potential is also computed. The operation count and our numerical experiments (see section below) show that in this case B_1 is approximately the same for the scalar harmonic FMM and velocity+stretching computations. Hence, only A_2 is changed in the case of the FMM for vortex methods. Eq. (38) then shows that the cost increase for a standard three potential representation will be $\sqrt{3}$ times, while for the two potential representation only $\sqrt{2}$ times, or that the latter method is $\sqrt{3/2} \approx 1.22$ times faster than the former method. Note then that in practice the depth of the octree can be changed only discretely, and a perfect balance of the sparse and dense parts of the algorithm cannot be achieved, so some fluctuations around the value $\sqrt{2}$ are expected. Analysis of efficiency of implementations with fine and coarse grained parallelism, such as [18], also can be done, but this requires particular architecture considerations, which goes beyond the scope of this paper.

4.2 Modification of complex valued harmonic FMM

It is proposed in [13] to modify an available FMM routine for complex valued harmonic function to an FMM routine which provides the FMM for real valued biharmonic functions. So just one complex FMM can be executed instead of two FMMs for the real functions. Our tests show that such an approach provides a

small advantage compared to the FMMs for real harmonic functions. This method can be taken and applied directly to the present case, since a complex valued harmonic function $\Psi(\mathbf{r})$ can be composed from two real functions $\phi(\mathbf{r})$ and $\chi(\mathbf{r})$, as

$$\Psi(\mathbf{r}) = \phi(\mathbf{r}) + i\chi(\mathbf{r}). \tag{39}$$

Further the translation algorithm for $\Psi(\mathbf{r})$ will be exactly the same as for the biharmonic functions, described in [13], with the only difference in the conversion operators.

4.3 Generation of multipole expansions

Here we propose two methods to generate multipole expansions. The first method requires just a slight modification of a function generating the multipole expansion of a dipole source, which are available in many harmonic FMM codes. The second method utilizes a function generating the multipole expansion of a monopole source.

4.3.1 Method 1

Consider multipole expansion of $\mathbf{v}_l(\mathbf{y})$ given by Eq. (1) about the center, $\mathbf{x}_*$,of a source box b containing $\mathbf{x}_l$ and denote $\mathbf{r} = \mathbf{y} - \mathbf{x}_*$, $\mathbf{r}_l = \mathbf{x}_l - \mathbf{x}_*$. The purpose is to find coefficients of scalar potentials ϕ_{ln}^m and χ_{ln}^m, which then should be summed up with respect to l, $\mathbf{x}_l \in b$ to obtain coefficients $\phi_{(b)n}^m$ and $\chi_{(b)n}^m$ for the box, which further should be used in the translation process.

It is not difficult to show that the auxiliary harmonic functions

$$\psi_l = \mathbf{r}\cdot\nabla\phi_l = \mathcal{D}_{\mathbf{r}}\phi_l, \quad \varpi_l = \chi_l + \mathbf{r}\cdot\nabla\chi_l = (\mathcal{I} + \mathcal{D}_{\mathbf{r}})\chi_l, \tag{40}$$

are dipoles,

$$\psi_l = \mathbf{r}\cdot\nabla\times\frac{\boldsymbol{\omega}_l}{|\mathbf{r}-\mathbf{r}_l|} = (\mathbf{r}_l\times\boldsymbol{\omega}_l)\cdot\left(\frac{\mathbf{r}-\mathbf{r}_l}{|\mathbf{r}-\mathbf{r}_l|^3}\right), \tag{41}$$

$$\varpi_l = \nabla\cdot\frac{\boldsymbol{\omega}_l}{|\mathbf{r}-\mathbf{r}_l|} = \frac{-\boldsymbol{\omega}_l\cdot(\mathbf{r}-\mathbf{r}_l)}{|\mathbf{r}-\mathbf{r}_l|^3}, \tag{42}$$

i.e. ψ_l is a dipole with moment $\mathbf{p}_l = \mathbf{r}_l\times\boldsymbol{\omega}_l$, while ϖ_l is a dipole with moment $\mathbf{q}_l = -\boldsymbol{\omega}_l$. Hence, coefficients ψ_{ln}^m and ϖ_{ln}^m can be found using the dipole expansion procedure. We can determine coefficients ϕ_{ln}^m and χ_{ln}^m, as the operators in Eq. (40) are diagonal in the S basis (see Eqs (62) and (64)):

$$\phi_{ln}^m = -\frac{1}{n+1}\psi_{ln}^m, \quad \chi_{ln}^m = -\frac{1}{n}\varpi_{ln}^m, \quad \left(\chi_{l0}^0 = 0\right). \tag{43}$$

4.3.2 Method 2

Using Eq. (28), we obtain

$$\mathbf{v}_l(\mathbf{y}) = \nabla\times\frac{\boldsymbol{\omega}_l}{|\mathbf{r}-\mathbf{r}_l|} = \sum_{n=0}^{\infty}\sum_{m=-n}^{n} g_{ln}^m\mathbf{F}_{ln}^m(\mathbf{r}), \quad \mathbf{F}_{ln}^m(\mathbf{r}) = \nabla\times[\boldsymbol{\omega}_l S_n^m(\mathbf{r})], \quad g_{ln}^m = R_n^{-m}(-\mathbf{r}_l). \tag{44}$$

Note then that $\mathbf{F}_{ln}^m$ is equivalent to the right hand side of Eq. (16), where one should set $\mathbf{t} = \boldsymbol{\omega}_l$, $\widehat{\chi} = S_n^m(\mathbf{r})$. So this function can be represented in the form provided by the left hand side of Eq. (16), where functions ϕ' and χ' can be found from Eqs (21) and (23) i.e.

$$\begin{aligned} \mathbf{F}_{ln}^m(\mathbf{r}) &= \nabla \times [\boldsymbol{\omega}_l S_n^m(\mathbf{r})] = \nabla \Phi_{ln}^m(\mathbf{r}) + \nabla \times (\mathbf{r} X_{ln}^m(\mathbf{r})), \\ \Phi_{ln}^m(\mathbf{r}) &= \mathcal{C}_{12}(\boldsymbol{\omega}_l) S_n^m(\mathbf{r}), \quad X_{ln}^m(\mathbf{r}) = (\mathcal{C}_{22}(\boldsymbol{\omega}_l) - \mathcal{I}) S_n^m(\mathbf{r}). \end{aligned} \tag{45}$$

Substituting this into Eq. (44) and using representation of the conversion operators in the S basis, Eq. (75), we obtain

$$\begin{aligned} \mathbf{v}_l(\mathbf{y}) &= \nabla \phi_l(\mathbf{r}) + \nabla \times (\mathbf{r} \chi_l(\mathbf{r})), \\ \phi_l(\mathbf{r}) &= \sum_{n=0}^{\infty} \sum_{m=-n}^{n} g_{ln}^m \mathcal{C}_{12}(\boldsymbol{\omega}_l) S_n^m(\mathbf{r}) = \sum_{n=0}^{\infty} \sum_{m=-n}^{n} \phi_{ln}^m S_n^m(\mathbf{r}), \\ \chi_l(\mathbf{r}) &= \sum_{n=0}^{\infty} \sum_{m=-n}^{n} g_{ln}^m (\mathcal{C}_{22}(\boldsymbol{\omega}_l) - \mathcal{I}) S_n^m(\mathbf{r}) = \sum_{n=0}^{\infty} \sum_{m=-n}^{n} \chi_{ln}^m S_n^m(\mathbf{r}), \end{aligned} \tag{46}$$

where

$$\begin{aligned} \phi_{ln}^m &= \frac{1}{n+1}\left[(\omega_{lx} - i\omega_{ly})\frac{n-m+1}{2} g_{ln}^{m-1} - (\omega_{lx} + i\omega_{ly})\frac{n+m+1}{2} g_{ln}^{m+1} - i\omega_{lz} m g_{ln}^m\right], \\ \chi_{ln}^m &= -\frac{1}{n}\left[\frac{1}{2}(\omega_{ly} + i\omega_{lx}) g_{l,n-1}^{m-1} - \frac{1}{2}(\omega_{ly} - i\omega_{lx}) g_{l,n-1}^{m+1} - \omega_{lz} g_{l,n-1}^m\right], \quad \left(\chi_{l0}^0 = 0\right). \end{aligned} \tag{47}$$

4.4 Translations

In many FMM codes translations are performed using the rotation-coaxial translation-back rotation (RCR) decomposition of the translation operators, which reduces translation cost of expansions of length p^2 to $O(p^3)$, opposed to $O(p^4)$ required for the direct application of the translation matrix (e.g. see [13]). Such a decomposition is also beneficial for faster conversion, since the rotations do not change the form of decomposition of the vector field (5) and there is no need to rotate ϕ and χ in conversion operators. Coaxial translation means translation along the z direction to distance t, in which case expressions for the conversion operators (74) and (75) become even simpler ($\mathbf{t} = t\mathbf{i}_z$, $t_x = t_y = 0$, $t_z = t$):

$$\begin{aligned} &R \text{ conversion} : \quad \widetilde{\phi}_n^m = \widehat{\phi}_n^m + it\frac{m}{n}\widehat{\chi}_n^m, \quad \left(\widetilde{\phi}_0^0 = \widehat{\phi}_0^0\right), \quad \widetilde{\chi}_n^m = \widehat{\chi}_n^m - \frac{t}{n+1}\widehat{\chi}_{n+1}^m, \\ &S \text{ conversion} : \quad \widetilde{\phi}_n^m = \widehat{\phi}_n^m - it\frac{m}{n+1}\widehat{\chi}_n^m, \quad \widetilde{\chi}_n^m = \widehat{\chi}_n^m + \frac{t}{n}\widehat{\chi}_{n-1}^m, \quad \left(\widetilde{\chi}_0^0 = \widehat{\chi}_0^0\right). \end{aligned} \tag{48}$$

Figure 1 illustrates the present translation scheme which uses the RCR-decomposition (rotation-coaxial translation-back rotation).

4.5 Evaluation of local expansions

4.5.1 Velocity

As a result of the FMM downward pass the R expansions of scalar potentials are obtained about the center $\mathbf{y}_*$,of an evaluation box b containing receiver point $\mathbf{y}$

$$\phi(\mathbf{r}) = \sum_{n=0}^{\infty} \sum_{m=-n}^{n} \phi_n^m R_n^m(\mathbf{r}), \quad \chi(\mathbf{r}) = \sum_{n=0}^{\infty} \sum_{m=-n}^{n} \chi_n^m R_n^m(\mathbf{r}), \quad \mathbf{r} = \mathbf{y} - \mathbf{y}_*. \tag{49}$$

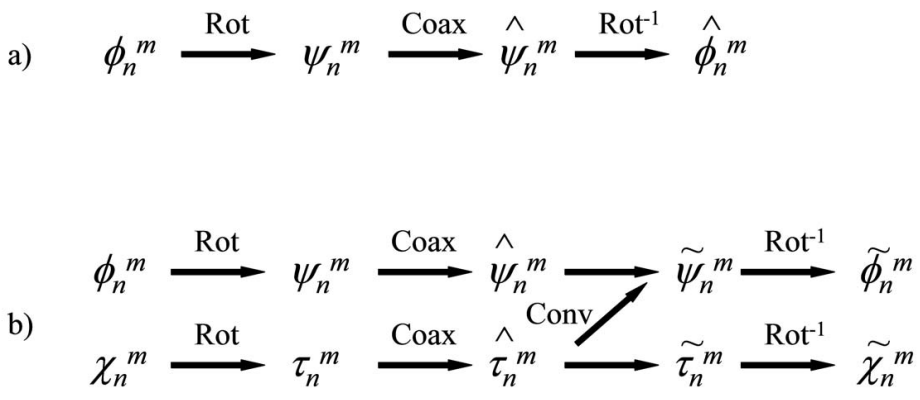


Figure 1: Translation schemes for the FMM for the scalar Laplace equation (a), and the FMM for the DCVLE (b), based on the RCR-decomposition. The operators are shown abbreviated as follows: Rot: rotation, Coax: coaxial translation, Rot^{-1}: back (inverse) rotation.

Cartesian components of the velocity can be obtained by projection of Eq. (5) to the basis vectors $\mathbf{i}_x, \mathbf{i}_y$, and $\mathbf{i}_z$ as follows

$$v_k = \mathbf{i}_k \cdot \mathbf{v} = \mathbf{i}_k \cdot \nabla\phi + \mathbf{i}_k \cdot \nabla \times (\mathbf{r}\chi) = \mathcal{D}_{\mathbf{i}_k}\phi + \mathcal{D}_{\mathbf{r}\times\mathbf{i}_k}\chi, \quad k = x, y, z. \tag{50}$$

since $\mathbf{i}_k \cdot \nabla \times (\mathbf{r}\chi) = \mathbf{i}_k \cdot (\nabla\chi \times \mathbf{r}) = (\mathbf{r} \times \mathbf{i}_k) \cdot \nabla\chi$. Using representations of the above operators in the R basis, (67) and (73), where $\mathbf{t} = \mathbf{i}_k$, we determine

$$\begin{aligned}
v_k &= \sum_{n=0}^{\infty}\sum_{m=-n}^{n} v_{kn}^m R_n^m(\mathbf{r}), \quad k = x, y, z, \\
v_{xn}^m &= \frac{1}{2}\left[i\phi_{n+1}^{m-1} + i\phi_{n+1}^{m+1} + (n-m)\,\chi_n^{m+1} - (n+m)\,\chi_n^{m-1}\right], \\
v_{yn}^m &= \frac{1}{2}\left[\phi_{n+1}^{m-1} - \phi_{n+1}^{m+1} + i\,(n-m)\,\chi_n^{m+1} + i\,(n+m)\,\chi_n^{m-1}\right], \\
v_{zn}^m &= -\phi_{n+1}^m - im\chi_n^m.
\end{aligned} \tag{51}$$

4.5.2 Stretching term and strain tensor

Furthermore, consider computation of the vortex stretching at evaluation point $\mathbf{y}_j$ ($\mathbf{r}_j = \mathbf{y}_j - \mathbf{y}_*$), assuming that the strength vector at this point is $\boldsymbol{\omega}_j$. The stretching is a vector

$$\mathbf{s}_j = (\boldsymbol{\omega}_j \cdot \nabla)\,\mathbf{v}(\mathbf{r})\big|_{\mathbf{r}=\mathbf{r}_j} = \mathcal{D}_{\boldsymbol{\omega}_j}\mathbf{v}(\mathbf{r})\big|_{\mathbf{r}=\mathbf{r}_j} = \sum_k \mathbf{i}_k\,\mathcal{D}_{\boldsymbol{\omega}_j} v_k(\mathbf{r})\big|_{\mathbf{r}=\mathbf{r}_j}. \tag{52}$$

Hence, the Cartesian components of this vector can be obtained simply from computed coefficients v_{kn}^m, Eq. (51), to which sparse operator $\mathbf{D}_{\boldsymbol{\omega}_j}^{(R)}$ should be applied (see Eq. (67)):

$$\begin{aligned}
s_{jk} &= \sum_{n=0}^{\infty}\sum_{m=-n}^{n} s_{jkn}^m R_n^m(\mathbf{r}_j), \quad k = x, y, z, \\
s_{jkn}^m &= \frac{1}{2}\left[(\omega_{jy} + i\omega_{jx})\,v_{k,n+1}^{m-1} - (\omega_{jy} - i\omega_{jx})v_{k,n+1}^{m+1}\right] - \omega_{jz}v_{k,n+1}^m.
\end{aligned} \tag{53}$$

In practice, it is more efficient to compute expansion coefficients u^m_{lkn} for the functions $u_{lk} = \mathcal{D}_{\mathbf{i}_l} v_k$, $l, k = 1, 2, 3$, which do not depend on the evaluation point j and then form the coefficients s^m_{jkn} for each point as

$$s^m_{jkn} = \sum_{l=1}^{3} \omega_{jl} u^m_{lkn}. \tag{54}$$

Note that u_{lk} are components of the tensor $\nabla \mathbf{v}$. The contraction $\beta = \nabla \mathbf{v} : \nabla \mathbf{v}$ can then be computed (for compressible flows). Also, computation of $\nabla \mathbf{v}$ provides the strain tensor, which can be used for modeling complex fluids.

5 Numerical tests

For numerical tests we used our FMM software which employs RCR-decomposition of translation operators, and modified it for two harmonic functions. Conversion operators in the R or S basis were executed after coaxial translation operators, as shown in Fig. 1. Additional small modifications were used in the algorithm to compute R basis functions for real harmonic functions recursively, as presented in [15]. In contrast to [15] no optimizations of the algorithm were used (no GPU acceleration, standard 189 M2L translation stencils, no variable truncation number, etc.), as the main purpose of this paper was to provide a basic comparative performance and accuracy test of the method, with a basic implementation. Open MP parallelization was used, which for a 4 core PC provided parallelization efficiency close to 100 percent. Wall clock times reported below were measured on an Intel QX6780 (2.8 GHz) 4 core PC with 8GB RAM.

5.1 Error tests

The first test we conducted is related to the numerical errors of computation of the velocity and stretching term. Also for comparisons we executed the FMM for a single harmonic function and measured numerical errors in the evaluation of the potential and its gradient. There are two basic sources of errors. The first one is due to truncation of the infinite series. These errors are controlled by the truncation number p (the infinite series (29) were replaced by the first p^2 terms, $n = 0, ..., p-1$; $m = -n, ..., n$), which we varied in the tests. The second source of errors is due to the roundoff, which in our computations with double precision in the range of tested p were smaller than the truncation errors (the roundoff errors were observed for $p \gtrsim 25$). The basic test was performed for N sources/receivers distributed randomly and uniformly inside a cube. The error, ϵ_2, was measured in the L_2 relative norm based on 1000 points randomly selected from the source set. (Our previous tests using direct computations show that even 100 points provide sufficient confidence for the L_2-norm error, see [13].) For the reference solution the velocity field, stretching term, potential and gradient were computed directly.

Figure 2 illustrates behavior of the computed errors for the velocity and stretching term. For reference, the dependence of the respective errors in the harmonic potential and in its gradient are also shown. It is seen that starting with $p \approx 7$ spectral convergence is observed for all cases. It is also noticeable, that the errors in potential computations are substantially smaller than that for the gradient or higher derivative computations. There are two basic reasons for this. First, the effective truncation number for each derivative is smaller by one compared to the potential, and second that in the truncated term for the derivative an additional factor $\sim p$ appears.

5.2 Performance tests

For optimal FMM performance the depth of the octree $l_{\max}$ should be chosen to minimize the total execution time. For all reported test cases we conducted such an optimization. Some results of the profiling (wall

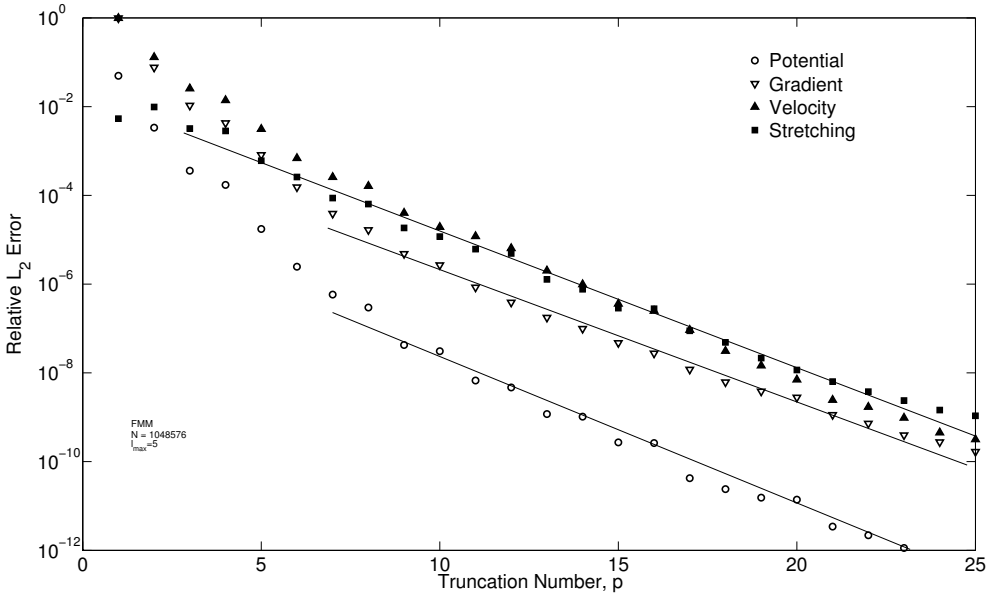


Figure 2: Dependences of the relative FMM errors in the L_2 norm on the truncation number, p. Errors were computed over 1000 random points for $N = 2^{20}$ sources of random intensity distributed uniformly randomly inside a cube. The maximum level of space subdivision $l_{\max} = 5$.

clock time in seconds) with random uniform distributions of sources inside a cube and on the surface of a sphere are provided in Tables 1 and 2. In these tables $\mathbf{v}$ and $\mathbf{s}$ indicate computations of the velocity and stretching term for vortical flows, while ϕ and $\nabla\phi$ refer to a reference case for the scalar Laplace equation, where the potential or both potential and its gradient should be computed. The total initialization time, which includes the data structure and precomputations related to translation operators can be amortized for a constant source/receiver set, and is reported separately from the total run time. As one can see this time is relatively small, while for dynamic problems it should be added to the total run time.

The times for the local sum ("sparse") and far field ("dense") matrix-vector products in the FMM are also reported. The latter is also expanded to show timing of the FMM stages. The truncation number for all cases was $p = 12$, which provides errors $\epsilon_2 \sim 10^{-5}$ for the velocity and stretching term computations, while smaller errors for ϕ and $\nabla\phi$ (see Fig. 2).

Table 2: Profiling of the FMM for random uniform distribution of sources inside a cube, $p = 12$.

Case	$l_{\max}$	Total Init	S-expansion	Upward	Downward	R-evaluation	Sparse MV	Total Run
$N = 2^{19}$								
$\mathbf{v}$ and $\mathbf{s}$	4	0.55	0.55	0.04	2.65	0.52	25.9	29.7
$\mathbf{v}$ alone	4	0.55	0.55	0.04	2.65	0.34	16.4	20.0
ϕ and $\nabla\phi$	5	1.20	0.20	0.12	10.7	0.36	3.95	15.3
ϕ alone	5	1.20	0.20	0.12	10.7	0.21	1.89	13.1
$N = 2^{20}$								
$\mathbf{v}$ and $\mathbf{s}$	5	1.71	1.05	0.27	25.3	1.11	14.2	41.9
$\mathbf{v}$ alone	5	1.71	1.05	0.27	25.3	0.59	9.04	36.3
ϕ and $\nabla\phi$	5	1.71	0.39	0.12	10.7	0.71	15.4	27.3
ϕ alone	5	1.71	0.39	0.12	10.7	0.43	7.32	19.0

Table 3: Profiling of the FMM for random uniform distribution of sources on a sphere surface, $p = 12$.

Case	$l_{\max}$	Total Init	S-expansion	Upward	Downward	R-evaluation	Sparse MV	Total Run
$N = 2^{19}$								
$\mathbf{v}$ and $\mathbf{s}$	7	1.23	0.88	0.34	9.48	0.66	3.75	15.1
$\mathbf{v}$ alone	6	0.66	0.63	0.10	2.46	0.34	8.66	12.2
ϕ and $\nabla\phi$	7	1.23	0.23	0.15	3.93	0.41	3.90	8.62
ϕ alone	7	1.23	0.23	0.15	3.93	0.26	1.86	6.43
$N = 2^{20}$								
$\mathbf{v}$ and $\mathbf{s}$	7	1.81	1.29	0.34	9.48	1.30	14.1	26.5
$\mathbf{v}$ alone	7	1.81	1.29	0.34	9.48	0.70	8.86	20.7
ϕ and $\nabla\phi$	7	1.81	0.46	0.15	4.14	0.84	15.3	20.9
ϕ alone	7	1.81	0.46	0.15	4.14	0.52	7.30	12.6

The tables show that in the cases when the number of translations for a single potential ϕ for the scalar Laplace equation and coupled potentials ϕ and χ for the DCVLE are the same (the same $l_{\max}$) the translation time for the latter case is approximately twice, as expected. Deviations may be explained by two factors. First, this is due to increase in the size of the arrays representing expansions and more time needed for data access, and, second, by the presence of the conversion operators. The tables also show that the time for sparse matrix-vector products for velocity only computations in DCVLE is slightly larger than for potential only computations in a harmonic FMM, while the time for the same operations for velocity and stretching computations are slightly smaller than for potential and gradient computations. Note, however, that if an additional near-field kernel should be computed, which may involve computation of special functions (exponents, error integrals, etc.) the time for the sparse matrix-vector product would increase, while the translation part would not be affected. Also note that, theoretically, in the optimized algorithm, an increase of the complexity of the sparse matrix-vector product by a factor of k affects the total complexity as $\sqrt{k}$ (see Eq. (38)). The ratio of the total time for the velocity and stretching computations to the time of potential and gradient computations depends on the problem. In all our numerical experiments this ratio never exceeded 2 (except for one outlier at $N = 1024$, see Fig. 4).

Figure 3 illustrates dependence of the wall clock time on the number of sources N, which in all cases was set to be equal to the number of receivers. It is seen that at large N the algorithm scales linearly, and the time for velocity and stretching term computations is always larger than that for scalar potential only computations by a factor of approximately two. Figure 4 illustrates the wall clock FMM run time ratio of velocity and stretching to potential and gradient computations for different p and $N = 2^k$, $k = 10, ..., 20$. It is seen that for $k > 11$ this ratio is larger than unity and smaller than two with a mean value about 1.405, while the average over all points shown in this figure is 1.423, which agrees well with theoretical value $\sqrt{2}$ (see discussion after Eq. (38)). Finally, we can see that the velocity and stretching computations are approximately twice as expensive as computation for a single harmonic potential. This also agrees well with the theory, since the cost of sparse matrix-vector product for a single harmonic potential approximately two times smaller than that for the velocity and stretching computations. Hence, in Eq. (38) both coefficients A_2 and B_1 for the latter case are two times larger than that for the former case, which provides exactly factor 2.

5.3 Example vortex computations

We implemented vortex particle and vortex filament methods (VPM and VFM, respectively) accelerated by the FMM described above. Some results for test problems related to the vortex ring dynamics are presented below.

In the VFM the total velocity field is a superposition of the Biot-Savart contour integrals taken along the

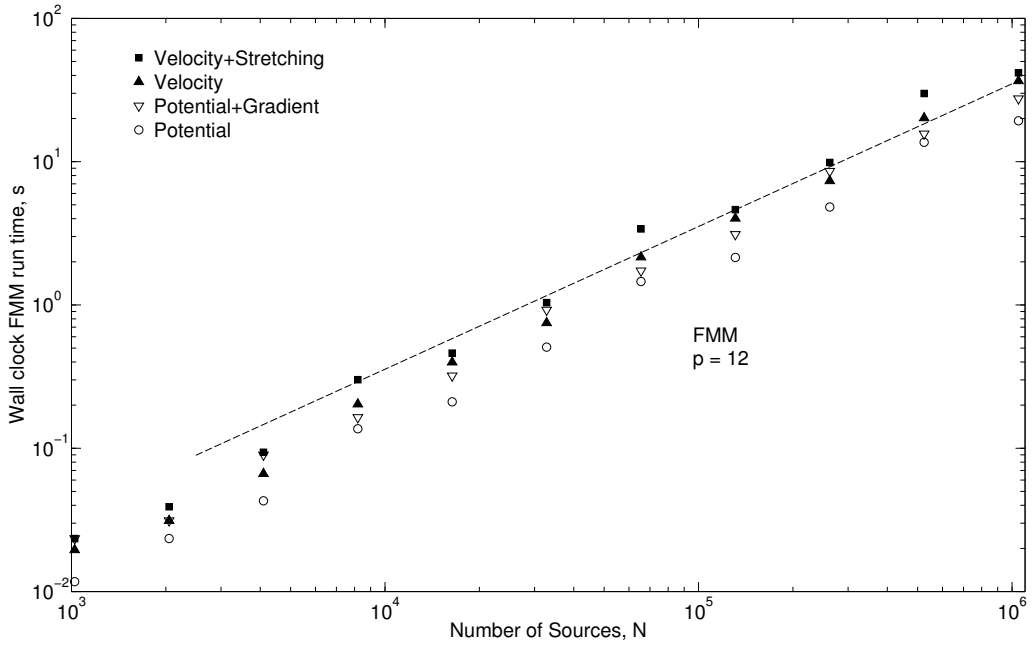


Figure 3: The wall clock time for the FMM for computation of vortical and potential flows (different terms and compinations). The straight line shows linear dependence. For all cases the sources are distributed randomly and uniformly inside a cube; the truncation number is constant, $p = 12$.

vortex filaments. The field of a single filament, C, can be discretized as

$$\begin{aligned} \mathbf{v}(\mathbf{y}) &= \frac{1}{4\pi}\int_C \frac{\Gamma(\mathbf{x})\, d\mathbf{l}(\mathbf{x}) \times (\mathbf{y}-\mathbf{x})}{|\mathbf{y}-\mathbf{x}|^3} = \sum_{i=1}^{N} \mathbf{v}_i(\mathbf{y}), \\ \mathbf{v}_i(\mathbf{y}) &= \frac{\Gamma_i}{4\pi}\int_{C_i} \frac{d\mathbf{l}(\mathbf{x}) \times (\mathbf{y}-\mathbf{x})}{|\mathbf{y}-\mathbf{x}|^3}, \quad C = \cup_{i=1}^{N} C_i, \end{aligned} \tag{55}$$

where N is the number of elements and each element C_i can be assumed a line segment of constant circulation Γ_i, in which case the integrals can be computed analytically (see Appendix B),

$$\mathbf{v}_i(\mathbf{y}) = \frac{\Gamma_i}{4\pi} \frac{\mathbf{r}_i^{(1)} \times \mathbf{r}_i^{(2)}}{r_i^{(1)} r_i^{(2)} + \mathbf{r}_i^{(1)} \cdot \mathbf{r}_i^{(2)}} \left(\frac{1}{r_i^{(1)}} + \frac{1}{r_i^{(2)}} \right), \quad \mathbf{r}_i^{(j)} = \mathbf{y} - \mathbf{x}_i^{(j)}, \quad r_i^{(j)} = \left| \mathbf{r}_i^{(j)} \right|, \quad j = 1, 2, \tag{56}$$

where $\mathbf{x}_i^{(j)}$, $j = 1, 2$, are coordinates of the end points of C_i and condition $\mathbf{v}_i(\mathbf{y}) = \mathbf{0}$ is imposed for $\mathbf{y} \in C_i$. Multipole expansion in terms of potentials ϕ and χ can be found using quadrature (see Appendix B). In the VFM vortex stretching occurs naturally since the ends of each segment propagate with the velocity of fluid particles at those points (e.g. see [4]). Hence in the FMM for the VFM the element centers are considered as "sources", while the end points are used as the "receivers".

For numerical examples we used the following smoothing kernel

$$K(r; a) = \operatorname{erf} \frac{r}{a\sqrt{2}} - \sqrt{\frac{2}{\pi}} \frac{r}{a} \exp\left(-\frac{r^2}{2a^2} \right), \tag{57}$$

which corresponds to the Gaussian vortex blob function with standard deviation a.

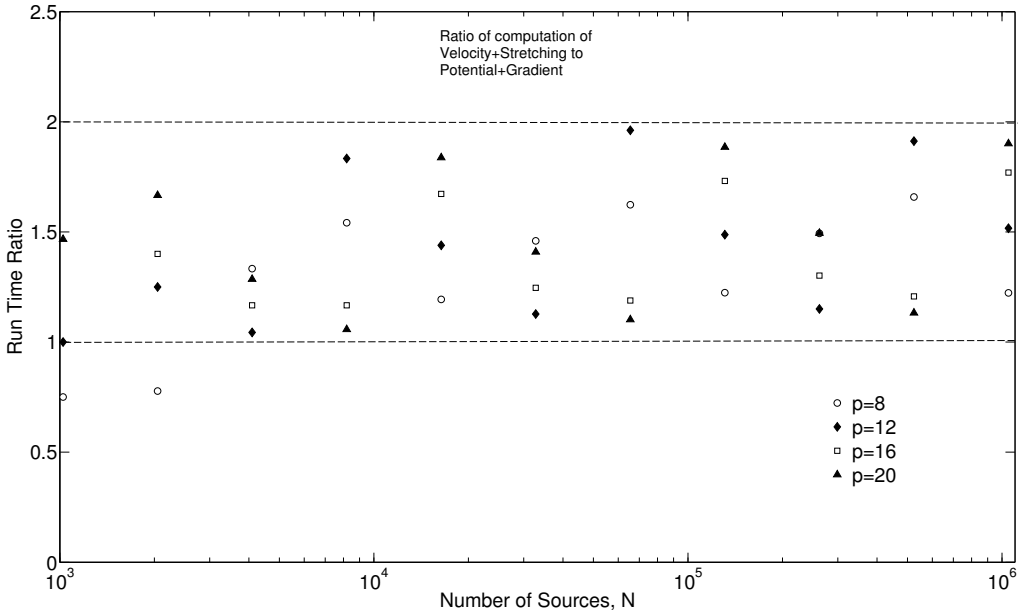


Figure 4: The ratio of the FMM run time for computation of the velocity and stretching term in a vortical flow to the respective time for the potential and gradient computations in a potential flow for different truncation numbers p and number of sources, N, which were randomly and uniformly distributed inside a cube. All data for $N > 2048$ are located between the dashed lines.

5.3.1 Single vortex ring computations

The self-induced motion of a vortex ring of radius R in an inviscid incompressible fluid is a classical solution [16, 20]. A characteristic of this problem is that the velocity of the ring itself should be infinitely large in this case, and the way to fix this is to introduce a small vortex core of size δ, in which case

$$V^{(self)} \sim \frac{\Gamma}{4\pi R}\left(\ln\frac{8R}{\delta} - \frac{1}{4}\right), \quad \delta \to 0. \tag{58}$$

The asymptotic behavior of the VFM scheme at large N can be estimated theoretically (see Appendix B).

$$V_\epsilon^{(self)} \sim \frac{\Gamma}{4\pi R}\ln\frac{2N}{\pi}, \quad N \to \infty. \tag{59}$$

In Fig. 5 we compared the velocity of the ring obtained via VFM and VPM (average of all vortex element velocities) with theoretical prediction (59). The ring velocity found via the VFM using the brute force method (no FMM) is about 1% different from the value provided by Eq. (59) and this difference decreases slowly with increasing N. So this error is not related to the use of the FMM, which at $p = 12$ and $p = 25$ are several orders smaller, and can be referred to the discretization scheme. Despite Eq. (81) provides consistency of the quadrature and FMM truncation errors it is sufficient to use $N_q = 2$ and even $N_q = 1$ at smaller p or very large N. This can be explained by the fact that the polygon approximation of the contour results in a globally non-smooth integrand. In this case high order quadratures do not improve accuracy, but the increase of the number of collocation points in a low order quadrature does. In the VPM we specified the characteristic vortex blob size in Eq. (57) as $a = 2\pi R/N_c$. For $N \ll N_c$ the vortex blobs do not overlap, while at $N \gg N_c$ the overlapping is high and we have a ring of constant radius $\delta \sim a$, which does not depend on N and so the ring has a constant velocity (58). We also computed the velocity field

using $N = 10^6$, $N_c = 5 \cdot 10^5$ for the VPM and $N \approx 5 \cdot 10^5$ for the VFM, which provides approximately the same ring velocity. At $p = 25$ the relative error between the numerical and analytical solutions (L_∞-norm) did not exceed $5 \cdot 10^{-9}$ (eight digits) for the distances larger than 2δ, where δ was found from Eq. (58).

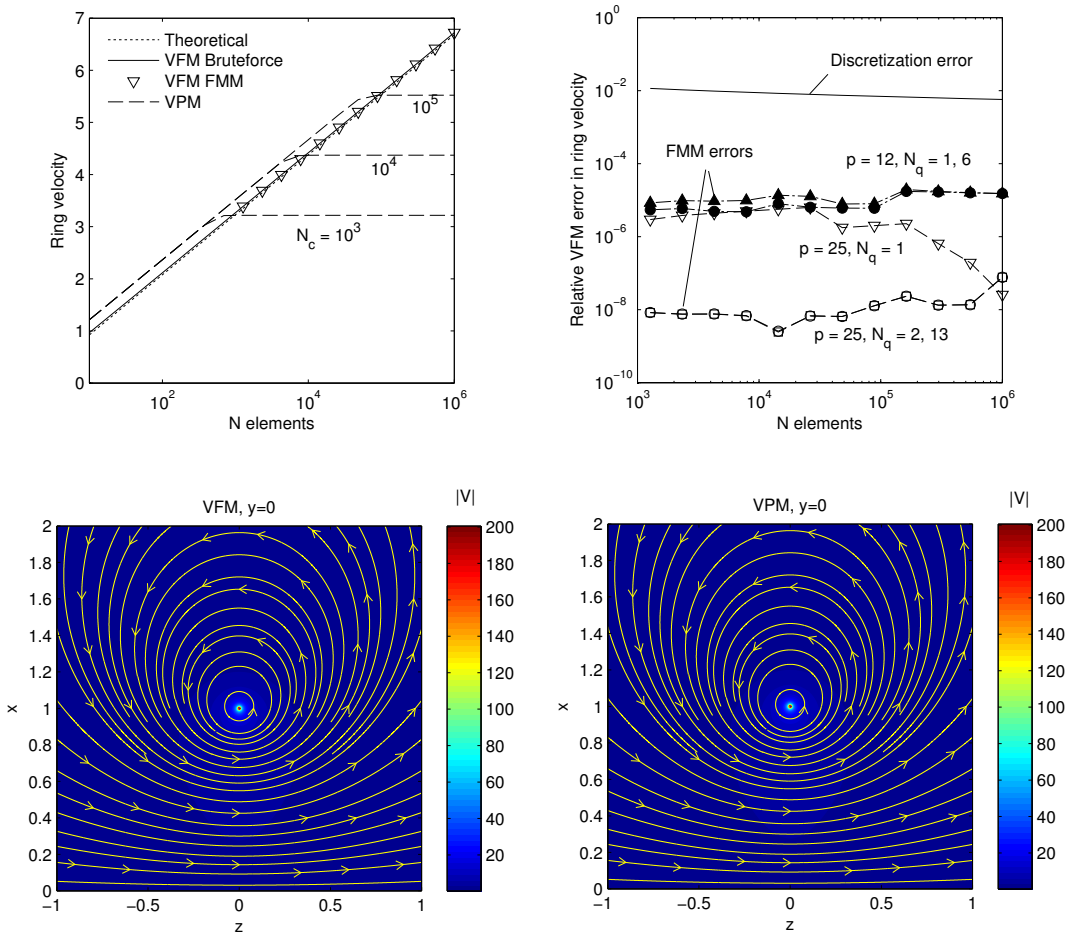


Figure 5: The dependences of the vortex ring velocity and computational errors on the number of discretization elements N obtained by the VFM and VPM (the top raw) and the respective velocity fields for $N = 10^6$ (VPM) and $N = 490960$ (VFM) (the bottom raw) for $R = 1$ and $\Gamma = 2\pi$. The theoretical velocity is given by Eq. (59). The dashed lines for the ring velocity correspond to the VPM computations with vortex particle size parameter $a = 2\pi R/N_c$, where N_c is shown near the curves. The errors are plotted for different parameters values of p and N_q controlling the accuracy of the FMM accelerated VFM. The discretization error is due to the approximation of the circle by linear elements and is not related to the FMM.

The brute force computations of the ring dynamics using the VFM or VPM are stable, since all vortex elements are in symmetric positions. However, the FMM errors introduce noise and asymmetry, which result in much faster development of instabilities. So for ring dynamics computations at each time step we applied a $O(N)$ stabilization procedure using a low-pass FFT-based filtering of the curve shape.

5.3.2 Pair of vortex rings

Motion along the z-axis of two vortex rings of radii $R_1(t)$ and $R_2(t)$ and positions $Z_1(t)$ and $Z_2(t)$ can be found from the solution of the initial value problem for the system of four ODEs

$$\frac{dR_j}{dt} = V_{3-j}^{(r)}(R_j, Z_j; R_{3-j}, Z_{3-j}), \quad \frac{dZ_j}{dt} = V_j^{(self)}(R_j) + V_{3-j}^{(z)}(R_j, Z_j; R_{3-j}, Z_{3-j}), \quad j = 1, 2, \quad (60)$$

where $V_j^{(r)}$ and $V_j^{(z)}$ are components of the velocity field $\mathbf{V}_j(r, z; R_j, Z_j)$ of the jth ring in cylindrical coordinates (r, z), and $V_j^{(self)}(R_j)$ is the self-induced velocity, Eq. (58). We integrated Eq. (60) using the 4th order Runge-Kutta method with controlled relative error 10^{-9}.

Numerical tests were performed for two cases with the same initial conditions $R_1(0) = R_2(0) = 1$, $Z_1(0) = 0$, $Z_2(0) = 0.1$ and ring core radii $\delta_1 = \delta_2 = \delta = 9.966931 \cdot 10^{-3}$, but different circulations $\Gamma_1 = -\Gamma_2 = 1$ and $\Gamma_1 = \Gamma_2 = 1$. The first case produces colliding rings, while the second case results in leapfrogging rings, shown in Figs 6 and 7. Vortex element simulations were performed using the VPM with $N = 5 \cdot 10^4$ elements per ring and blob size $a = 2\pi/N_c$, $N_c = 10^3$, which determines the ring core radii provided above during all computed times ($N_c \ll N$; for the colliding rings the initial radius increase was about 3 times at $t = t_{\max} \sim 0.4$). The time integration in the VPM was performed using a 4th order Runge-Kutta method with a constant time step $\Delta t = 5 \cdot 10^{-4}$ and an FFT-based low-pass shape filter (11 Fourier modes retained for each ring). In all cases we used the FMM with $p = 25$. All errors were measured as the maximum relative errors, ϵ_∞ (L_∞ norm). For the case of colliding rings positional (max of Z's and R's) error $\epsilon_\infty = 1.5 \cdot 10^{-3}$ for $0 \leqslant t \leqslant t_{\max}$, but $\epsilon_\infty = 1.4 \cdot 10^{-5}$ for $0 \leqslant t \leqslant t_1$ and $\epsilon_\infty = 1.2 \cdot 10^{-6}$ for $0 \leqslant t \leqslant t_2$, where at t_1 the ring cores touch ($Z_2 - Z_1 = 2\delta$) and at $t = t_2$ we have $Z_2 - Z_1 = 4\delta$. For the case of leapfrogging rings positional error $\epsilon_\infty < 6.2 \cdot 10^{-8}$. This shows that the FMM velocity computations are accurate and a larger error in the first case, presumably, has a non-FMM related nature (due to the Gaussian spread of the vortex blobs). Errors ϵ_∞ in the velocity fields in Figs 6 and 7 at distances larger than 2δ were approximately the same for both cases, $8.9 \cdot 10^{-5}$ and $1.7 \cdot 10^{-4}$, respectively.

6 Conclusion

The main goal of this study was to develop an efficient method for fast summation of elementary vortices. Numerical tests confirm the validity of the theory presented and efficiency of the method. Our numerical results show that one should expect an increase of the computation time by a factor of approximately two for the velocity and vorticity stretching term computations compared to a single harmonic function computations for the same FMM octree and the truncation number. Compared to potential and gradient computations for the scalar Laplace equation this increase varies in the range from 1 to 2 times (average ≈ 1.4) depending on particular source/receiver distribution, truncation number, etc. These numbers are in a good agreement with the theoretical FMM cost estimates.

An interesting observation from the study is that a general reconstruction of vector fields from given curl and divergence can be obtained via the present method, which operates only with two scalar potentials. This may have application to many other fields of physics, including plasma physics, electromagnetism, etc. In this sense the DCVLE appears to be a fundamental equation, the solutions of which can be accelerated via the harmonic FMM. As is shown, modifications of standard FMM programs are relatively easy, and require tracking of two harmonic functions, and implementation of the conversion operators used in each translation. Such operators are very sparse and simple (especially for the case of the RCR-decomposition) and their execution does not create substantial overheads. In terms of further acceleration of computations it is natural to consider implementations of the method on graphics processors (GPUs) for which the vortex methods are developed and tested (e.g. [25]).

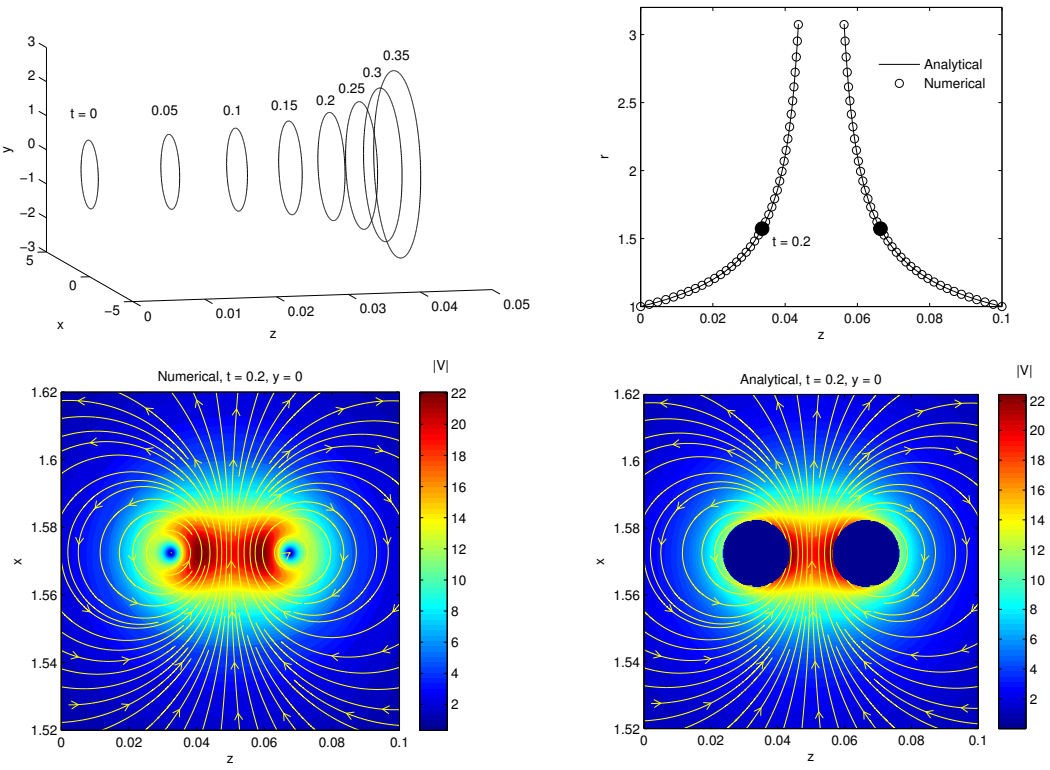


Figure 6: A comparison of dynamics of colliding rings ($\Gamma_1 = -\Gamma_2 = 1$), obtained by the VPM accelerated by the FMM ($p = 25$) with analytical solution. Only ring 1 is shown in the upper left picture. The velocity fields near the ring cores are shown for $t = 0.2$. In the plot of analytical solution the velocity field is zeroed within the core radius $\delta \approx 10^{-2}$ to show the radius.

We also conducted some tests for the vortex filament and vortex particle methods using the algorithm developed. These tests show a good accuracy of computations compared to analytical solutions and indicate that the FMM errors are typically much smaller than the errors of the VFM and VPM schemes introduced by line integral discretization, vortex blob representation, time integration errors, and interpolation procedures. The FMM brings the entire VEM method to $O(N)$ complexity for highly clustered non-uniform data distributions (e.g. vortex lines and sheets). Such acceleration is important for numerous practical applications, e.g. for computation of vortical fields generated by helicopters [17], while for such large scale simulations further study is required.

7 Acknowledgement

Work partially supported by AFOSR under MURI Grant W911NF0410176 (PI Dr. J. G. Leishman, monitor Dr. D. Smith); and by Fantalgo, LLC.

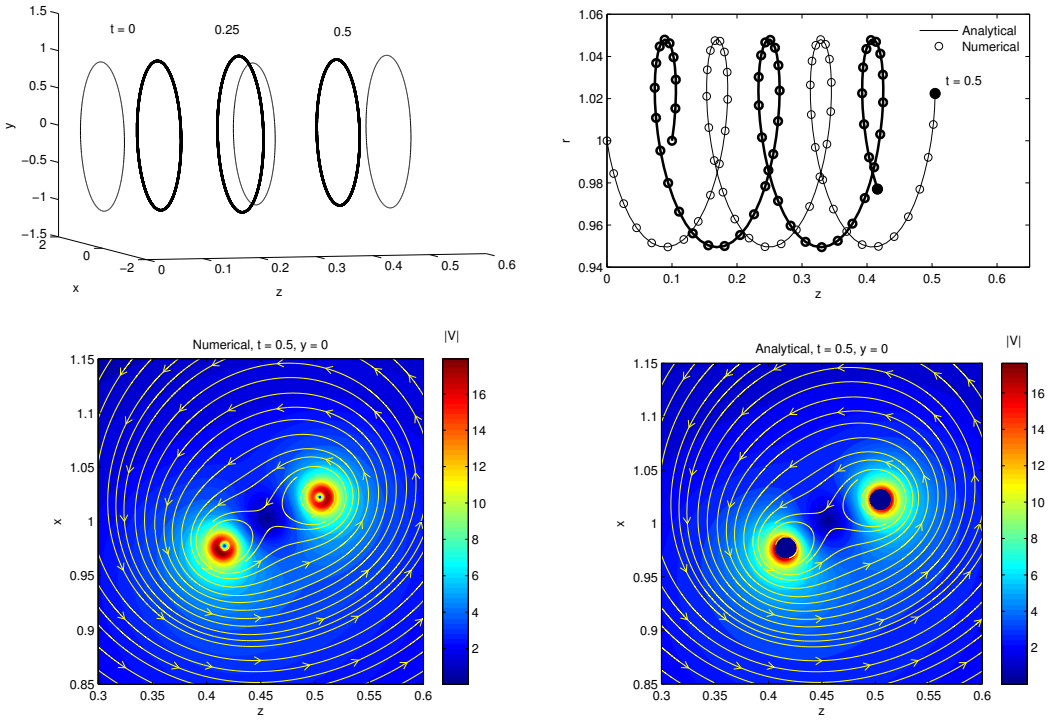


Figure 7: The same as in Fig. 6, but for leapfrogging rings ($\Gamma_1 = \Gamma_2 = 1$). In the upper raw of pictures the data for ring #1 are plotted by the thin lines and markers, while the data for ring #2 are plotted by the thick lines and markers.

References

[1] M. Abramowitz and I.A. Stegun, *Handbook of Mathematical Functions*, National Bureau of Standards, Washington, D.C., 1972.

[2] G.K. Batchelor, *An Introduction to Fluid Dynamics*, Cambridge University Press, Cambridge, 1967.

[3] H. Cheng, L. Greengard, and V. Rokhlin, "A fast adaptive multipole algorithm in three dimensions," J. Comput. Phys., 155:468–498, 1999.

[4] G.-H. Cottet and P.D. Koumoutsakos, *Vortex Methods*, Cambridge University Press, Cambridge, 2000.

[5] J.D. Eldredge, T. Colonius, and A. Leonard, "A vortex particle method for two-dimensional compressible flow," J. Comput. Phys., 179:371-399, 2002.

[6] M A. Epton and B. Dembart, "Multipole translation theory for the three-dimensional Laplace and Helmholtz equations," SIAM J. Sci. Comput., 16:865-897, 1995.

[7] Y. Fu and G.J. Rodin, "Fast solution methods for three-dimensional Stokesian many-particle problems," Commun. Numer. Meth. En., 16:145-149, 2000.

[8] L. Greengard and V. Rokhlin, "A fast algorithm for particle simulations," Journal of Computational Physics, 73:325-348, 1987.

[9] L. Greengard and V. Rokhlin, "A new version of the fast multipole method for the Laplace equation in three dimensions," Acta Numerica 6:229-269, 1997.

[10] N.A. Gumerov and R. Duraiswami, "Recursions for the computation of multipole translation and rotation coefficients for the 3-D Helmholtz equation," SIAM J. Sci. Comput., 25:1344–1381, 2003.

[11] N.A. Gumerov and R. Duraiswami, *Fast Multipole Methods for the Helmholtz Equation in Three Dimensions*, Elsevier, Oxford, 2005.

[12] N.A. Gumerov and R. Duraiswami, "Comparison of the efficiency of translation operators used in the fast multipole method for the 3D Laplace equation," Technical Report CS-TR-4701 and UMIACS-TR 2005-09, University of Maryland Department of Computer Science and Institute for Advanced Computer Studies, Nov. 2005.

[13] N.A. Gumerov and R. Duraiswami, "Fast multipole method for the biharmonic equation in three dimensions," J. Comput. Phys., 215:363–383, 2006.

[14] N.A. Gumerov and R. Duraiswami, "A scalar potential formulation and translation theory for the time-harmonic Maxwell equations," J. Comput. Phys., 225:206–236, 2007.

[15] N.A. Gumerov and R. Duraiswami, "Fast multipole methods on graphics processors," J. Comput. Phys., 227:8290-8313, 2008.

[16] H. Helmholtz, "On integrals of the hydrodynamic equations which express vortex motion," Phil. Mag., 33:485-512, 1867.

[17] Q. Hu, M. Syal, N.A. Gumerov, R. Duraiswami, and J. G. Leishman, "Toward improved aeromechanics simulations using recent advancements in scientific computing, " in Proceedings 67th Annual Forum of the American Helicopter Society, May 3-5 2011.

[18] Q. Hu, N.A. Gumerov, and R. Duraiswami, "Scalable fast multipole methods on distributed heterogeneous architectures," SC'11, International Conference for High Performance Computing, Networking, Storage, and Analysis, Seattle, WA, November 12-18, 2011.

[19] P. Koumoutsakos, "Multiscale flow simulations using particles," Annu. Rev. Fluid Mech., 37:457–87, 2005.

[20] H. Lamb, *Hydrodynamics*, Cambridge University Press, Cambridge, 1932.

[21] A.S. Sangani and G. Mo, "An O(N) algorithm for Stokes and Laplace interactions of particles," Phys. Fluids, 8:1990-2010, 1996.

[22] A.K. Tornberg and L. Greengard, "A fast multipole method for the three-dimensional Stokes equations," J. Comput. Phys., 227:1613-1619, 2008.

[23] G.S. Winckelmans and A. Leonard, "Contributions to vortex particle methods for the computation of three-dimensional incompressible unsteady flows," J. Comput. Phys., 109:247-273, 1993.

[24] G.Winckelmans, R. Cocle, L. Dufresne, and R. Capart, "Vortex methods and their application to trailing wake vortex simulations," C.R. Physique 6:467-486, 2005.

[25] R. Yokota, T. Narumi, R. Sakamaki, S. Kameoka, S. Obi, and K. Yasuoka, "Fast multipole methods on a cluster of GPUs for the meshless simulation of turbulence," Computer Physics Communications 180:2066-2078, 2009.

A Matrix representation of differential and conversion operators

A.1 Operator $\mathcal{D}_{\mathbf{r}}$

To obtain the representation of this operator there is no need to consider differential relations, since according to definition (10) we have $\mathcal{D}_{\mathbf{r}} = r\left(\partial/\partial r\right)$ and from Eq. (25) we have

$$\mathcal{D}_{\mathbf{r}} R_n^m\left(\mathbf{r}\right) = nR_n^m\left(\mathbf{r}\right), \quad \mathcal{D}_{\mathbf{r}} S_n^m\left(\mathbf{r}\right) = -\left(n+1\right) S_n^m\left(\mathbf{r}\right), \quad n = 0, 1, ... \tag{61}$$

This shows that matrices $\mathbf{D}_{\mathbf{r}}^{(R)}$ and $\mathbf{D}_{\mathbf{r}}^{(S)}$ representing this operator are diagonal and have entries

$$\left(\mathbf{D}_{\mathbf{r}}^{(R)}\right)_{nn'}^{mm'} = n\delta_{mm'}\delta_{nn'}, \quad \left(\mathbf{D}_{\mathbf{r}}^{(S)}\right)_{nn'}^{mm'} = -\left(n+1\right)\delta_{mm'}\delta_{nn'}, \quad n = 0, 1, ... \tag{62}$$

where $\delta_{mm'}$ is the Kronecker symbol.

Conversion operators (23) contain inverse operators $\mathcal{D}_{\mathbf{r}}^{-1}$ and $\left(\mathcal{I} + \mathcal{D}_{\mathbf{r}}\right)^{-1}$, which also are diagonal. It may be a cause for concern for the inverse operators that zeros appear on the diagonal of matrix $\mathbf{D}_{\mathbf{r}}^{(R)}$ and on the diagonal of matrix $\mathbf{I} + \mathbf{D}_{\mathbf{r}}^{(S)}$ at $n = 0$. However, these are easily dispensed with. For the former case we note that harmonic $n = 0$ corresponds to a constant basis function $R_0^0\left(\mathbf{r}\right)$. Eq. (22) shows that this affects only the constant added to potential ϕ, which obviously does not affect the velocity field (5), and can be set to an arbitrary value, e.g. to zero. For the latter case, Eq. (11) shows that harmonic $n = 0$ in multipole expansion of function χ also does not affect the velocity field, since

$$\nabla \times \left(\mathbf{r} r^{-1}\right) = -\mathbf{r} \times \nabla\left(r^{-1}\right) = r^{-2}\mathbf{r} \times \mathbf{r} = \mathbf{0}. \tag{63}$$

Since operator $\left(\mathbf{I}+\mathbf{D}_{\mathbf{r}}^{(S)}\right)^{-1}$ is needed only to determine converted function χ (see Eq. (22) this also can be set to zero. In other words, for the purpose of computation of the conversion operators the inverse operators for singular matrices can be defined as follows

$$\left[\left(\mathbf{D}_{\mathbf{r}}^{(R)}\right)^{-1}\right]_{nn'}^{mm'}=\delta_{mm'}\delta_{nn'}\left\{\begin{array}{cc} n^{-1}, & n>0 \\ 0, & n=0 \end{array}\right. , \quad \left[\left(\mathbf{I}+\mathbf{D}_{\mathbf{r}}^{(S)}\right)^{-1}\right]_{nn'}^{mm'}=\delta_{mm'}\delta_{nn'}\left\{\begin{array}{cc} -n^{-1}, & n>0 \\ 0, & n=0 \end{array}\right. . \tag{64}$$

A.2 Operator $\mathcal{D}_{\mathbf{t}}$

From definitions (10) and (35) we have

$$\mathcal{D}_{\mathbf{t}}=t_x\frac{\partial}{\partial x}+t_y\frac{\partial}{\partial y}+t_z\frac{\partial}{\partial z}=\frac{1}{2}\left[\left(t_x-it_y\right)\mathcal{D}_{x+iy}+\left(t_x+it_y\right)\mathcal{D}_{x-iy}\right]+t_z\mathcal{D}_z. \tag{65}$$

Using Eq. (34) we obtain

$$\begin{aligned}\mathcal{D}_{\mathbf{t}}R_n^m &= \frac{1}{2}\left[\left(t_y+it_x\right)R_{n-1}^{m+1}-\left(t_y-it_x\right)R_{n-1}^{m-1}\right]-t_zR_{n-1}^m, \\ \mathcal{D}_{\mathbf{t}}S_n^m &= \frac{1}{2}\left[\left(t_y+it_x\right)S_{n+1}^{m+1}-\left(t_y-it_x\right)S_{n+1}^{m-1}\right]-t_zS_{n+1}^m.\end{aligned} \tag{66}$$

Taking into account that matrices $\mathbf{D}_{\mathbf{t}}^{(R)}$ and $\mathbf{D}_{\mathbf{t}}^{(S)}$ are transposed to the reexpansion matrices, we obtain

$$\begin{aligned}\left(\mathbf{D}_{\mathbf{t}}^{(R)}\right)_{nn'}^{mm'} &= \delta_{n+1,n'}\left[\frac{1}{2}\left(t_y+it_x\right)\delta_{m-1,m'}-\frac{1}{2}\left(t_y-it_x\right)\delta_{m+1,m'}-t_z\delta_{mm'}\right], \\ \left(\mathbf{D}_{\mathbf{t}}^{(S)}\right)_{nn'}^{mm'} &= \delta_{n-1,n'}\left[\frac{1}{2}\left(t_y+it_x\right)\delta_{m-1,m'}-\frac{1}{2}\left(t_y-it_x\right)\delta_{m+1,m'}-t_z\delta_{mm'}\right].\end{aligned} \tag{67}$$

A.3 Operator $\mathcal{D}_{\mathbf{r}\times\mathbf{t}}$

From definitions (10) and (35) we have

$$\begin{aligned}\mathcal{D}_{\mathbf{r}\times\mathbf{t}} &= \left(yt_z-zt_y\right)\frac{\partial}{\partial x}+\left(zt_x-xt_z\right)\frac{\partial}{\partial y}+\left(xt_y-yt_x\right)\frac{\partial}{\partial z} \\ &= -i(t_x+it_y)\left[\xi_-\mathcal{D}_z-\frac{1}{2}z\mathcal{D}_{x-iy}\right]+i(t_x-it_y)\left[\xi_+\mathcal{D}_z-\frac{1}{2}z\mathcal{D}_{x+iy}\right]+it_z\left[\xi_-\mathcal{D}_{x+iy}-\xi_+\mathcal{D}_{x-iy}\right], \\ \xi_\pm &= \frac{x\pm iy}{2}.\end{aligned} \tag{68}$$

Consider first action of this operator on basis functions $R_n^m\left(\mathbf{r}\right)$. The following relations derived in [13] are useful in this case:

$$\begin{aligned}\xi_+R_n^m &= -i\frac{n+m+2}{2}R_{n+1}^{m+1}-\frac{i}{2}zR_n^{m+1}, \\ \xi_-R_n^m &= -i\frac{n-m+2}{2}R_{n+1}^{m-1}-\frac{i}{2}zR_n^{m-1}.\end{aligned} \tag{69}$$

We have then, using these relations and Eq. (34)

$$\begin{aligned}\left[\xi_-\mathcal{D}_z-\frac{1}{2}z\mathcal{D}_{x-iy}\right]R_n^m &= -\xi_-R_{n-1}^m-\frac{1}{2}izR_{n-1}^{m-1}=i\frac{n-m+1}{2}R_n^{m-1}, \\ \left[\xi_+\mathcal{D}_z-\frac{1}{2}z\mathcal{D}_{x+iy}\right]R_n^m &= -\xi_+R_{n-1}^m-\frac{1}{2}izR_{n-1}^{m+1}=i\frac{n+m+1}{2}R_n^{m+1}, \\ \left[\xi_-\mathcal{D}_{x+iy}-\xi_+\mathcal{D}_{x-iy}\right]R_n^m &= i\xi_-R_{n-1}^{m+1}-i\xi_+R_{n-1}^{m-1}=-mR_n^m.\end{aligned} \tag{70}$$

Now we obtain from Eq. (68)

$$\mathcal{D}_{\mathbf{r}\times\mathbf{t}}R_n^m = (t_x+it_y)\frac{n-m+1}{2}R_n^{m-1} - (t_x-it_y)\frac{n+m+1}{2}R_n^{m+1} - it_z m R_n^m. \tag{71}$$

To get a similar relation for basis functions $S_n^m(\mathbf{r})$ we can use relation (27). Using identity $(\mathbf{r}\times\mathbf{t})\cdot\nabla\left[f(r)\,g(\mathbf{r})\right] = f(r)\,(\mathbf{r}\times\mathbf{t})\cdot\nabla g(\mathbf{r})$ and Eq. (71), we obtain

$$\begin{aligned}\mathcal{D}_{\mathbf{r}\times\mathbf{t}}S_n^m &= (-1)^{n+m}(n-m)!(n+m)!r^{-2n-1}\mathcal{D}_{\mathbf{r}\times\mathbf{t}}R_n^m \\ &= -(t_x+it_y)\frac{n+m}{2}S_n^{m-1} + (t_x-it_y)\frac{n-m}{2}S_n^{m+1} - it_z m S_n^m.\end{aligned} \tag{72}$$

Expressions for the representing matrices for the local and multipole bases follow from Eqs (71) and (72):

$$\begin{aligned}\left(\mathbf{D}_{\mathbf{r}\times\mathbf{t}}^{(R)}\right)_{nn'}^{mm'} &= \delta_{nn'}\left[(t_x+it_y)\frac{n'-m'+1}{2}\delta_{m+1,m'} - (t_x-it_y)\frac{n'+m'+1}{2}\delta_{m-1,m'} - it_z m'\delta_{mm'}\right], \\ \left(\mathbf{D}_{\mathbf{r}\times\mathbf{t}}^{(S)}\right)_{nn'}^{mm'} &= \delta_{nn'}\left[-(t_x+it_y)\frac{n'+m'}{2}\delta_{m+1,m'} + (t_x-it_y)\frac{n'-m'}{2}\delta_{m-1,m'} - it_z m'\delta_{mm'}\right].\end{aligned} \tag{73}$$

A.4 Conversion operators

It is not difficult to obtain matrix representations for the conversion operator from Eqs (14) and (23) and expressions for the differential operators derived above. A more compact form relating the expansion coefficients of functions in Eq. (22) for the R expansions is

$$\begin{aligned}\widetilde{\phi}_n^m &= \widehat{\phi}_n^m - \frac{1}{n}\left[(t_x+it_y)\frac{n-m}{2}\widehat{\chi}_n^{m+1} - (t_x-it_y)\frac{n+m}{2}\widehat{\chi}_n^{m-1} - it_z m\widehat{\chi}_n^m\right], \quad \left(\widetilde{\phi}_0^0 = \widehat{\phi}_0^0\right) \\ \widetilde{\chi}_n^m &= \widehat{\chi}_n^m + \frac{1}{n+1}\left[\frac{1}{2}(t_y+it_x)\widehat{\chi}_{n+1}^{m-1} - \frac{1}{2}(t_y-it_x)\widehat{\chi}_{n+1}^{m+1} - t_z\widehat{\chi}_{n+1}^m\right].\end{aligned} \tag{74}$$

Similarly, for the S expansions we have

$$\begin{aligned}\widetilde{\phi}_n^m &= \widehat{\phi}_n^m + \frac{1}{n+1}\left[-(t_x+it_y)\frac{n+m+1}{2}\widehat{\chi}_n^{m+1} + (t_x-it_y)\frac{n-m+1}{2}\widehat{\chi}_n^{m-1} - it_z m\widehat{\chi}_n^m\right] \\ \widetilde{\chi}_n^m &= \widehat{\chi}_n^m - \frac{1}{n}\left[\frac{1}{2}(t_y+it_x)\widehat{\chi}_{n-1}^{m-1} - \frac{1}{2}(t_y-it_x)\widehat{\chi}_{n-1}^{m+1} - t_z\widehat{\chi}_{n-1}^m\right], \quad \left(\widetilde{\chi}_0^0 = \widehat{\chi}_0^0\right).\end{aligned} \tag{75}$$

B Some line integrals

B.1 Velocity field of linear element

Consider velocity field, Eq. (55), of a linear vortex element of constant circulation Γ with end points $\mathbf{x}^{(1)}$ and $\mathbf{x}^{(2)}$. This integral diverges for $\mathbf{y}\in C$. For $\mathbf{y}\notin C$ we change the integration variable as

$$\mathbf{x} = \mathbf{x}^{(c)} + \frac{1}{2}\mathbf{l}\xi, \quad \mathbf{x}^{(c)} = \frac{1}{2}\left(\mathbf{x}^{(2)}+\mathbf{x}^{(1)}\right), \quad \mathbf{l} = \mathbf{x}^{(2)}-\mathbf{x}^{(1)}, \quad d\mathbf{l}(\mathbf{x}) = \frac{1}{2}\mathbf{l}d\xi, \tag{76}$$

to obtain

$$\mathbf{v}(\mathbf{y}) = \frac{\Gamma}{8\pi}\mathbf{l}\times\left(\mathbf{y}-\mathbf{x}^{(c)}\right)\int_{-1}^{1}\frac{d\xi}{\left|\mathbf{y}-\mathbf{x}^{(c)}+\frac{1}{2}\mathbf{l}\xi\right|^3}. \tag{77}$$

The definite integral here can be computed using the primitive (can be checked by differentiation)

$$\int \frac{d\xi}{|\mathbf{a}+\mathbf{b}\xi|^3} = \frac{b^2\xi + (\mathbf{a}\cdot\mathbf{b})}{\left[a^2b^2 - (\mathbf{a}\cdot\mathbf{b})^2\right]|\mathbf{a}+\mathbf{b}\xi|} + C, \quad a = |\mathbf{a}|, \quad b = |\mathbf{b}|. \tag{78}$$

Further we note that all vectors in the resulting formula according to Eq. (76) can be expressed in terms of $\mathbf{r}^{(1)} = \mathbf{y} - \mathbf{x}^{(1)}$ and $\mathbf{r}^{(2)} = \mathbf{y} - \mathbf{x}^{(2)}$, which results in expression (56).

B.2 Far field expansions

Far field expansion of the integrand for elementary velocity field in Eq. (77) can be obtained similarly to derivation of Eq. (47) from Eq. (44). Indeed, we have for expansion center $\mathbf{x}_*$,

$$\begin{aligned} \mathbf{v}(\mathbf{y}) &= \int_{-1}^{1} \nabla \times \frac{\Gamma}{8\pi} \frac{\mathbf{l}d\xi}{|\mathbf{y} - \mathbf{x}^{(c)} + \frac{1}{2}\mathbf{l}\xi|} = \sum_{n=0}^{\infty} \sum_{m=-n}^{n} \widetilde{g}_n^m \mathbf{F}_n^m(\mathbf{r}), \\ \widetilde{g}_n^m &= \int_{-1}^{1} R_n^{-m}(-\mathbf{r}^{(c)} + \frac{1}{2}\mathbf{l}\xi) d\xi, \quad \mathbf{r} = \mathbf{y} - \mathbf{x}_*, \quad \mathbf{r}^{(c)} = \mathbf{x}^{(c)} - \mathbf{x}_*, \end{aligned} \tag{79}$$

Hence, Eqs (45) and (46) can be used to expand potentials ϕ and χ into the harmonic series. Coefficients of these series are provided by Eq. (47), where one simply should use $\frac{\Gamma}{8\pi}\mathbf{l}$ instead of vector $\boldsymbol{\omega}_l$ and coefficients $\widetilde{g}_n^m$ instead of g_{nl}^m. The problem then is to compute $\widetilde{g}_n^m$ in Eq. (79). These coefficients can be computed in a very straightforward way using Gauss-Legendre quadrature with weights w_j and abscissas ξ_j (see [1]),

$$\widetilde{g}_n^m = \sum_{j=1}^{N_q} w_j R_n^{-m}(-\mathbf{r}^{(c)} + \frac{1}{2}\mathbf{l}\xi_j). \tag{80}$$

Note now that functions $R_n^{-m}(-\mathbf{r}^{(c)} + \frac{1}{2}\mathbf{l}\xi)$ are polynomials of degree n of ξ (see [13]). Hence, the Gauss-Legendre quadrature (80) provides an exact result for $N_q > n/2$. Furthermore, for application of the FMM we truncate all series with p terms to provide a required accuracy. Therefore, the range of n needed is limited as $n \leqslant p-1$, and choice

$$N_q = \left[\frac{p-1}{2}\right] + 1, \tag{81}$$

provides an exact result for all harmonics needed for application of the FMM.

B.3 Velocity of the vortex ring without self-induction of small elements

We exclude an ϵ vicinity of a point $\mathbf{y}$ on the ring by putting its self-induction to zero. In this case we have

$$\mathbf{v}(\mathbf{y}) = \frac{\Gamma}{4\pi} \int_{C\setminus C_\epsilon} \frac{d\mathbf{l}(\mathbf{x}) \times (\mathbf{y} - \mathbf{x})}{|\mathbf{y} - \mathbf{x}|^3}. \tag{82}$$

Now for a ring in z plane and $\mathbf{y}$ located on the x axis we can express Cartesian coordinates of vectors in Eq. (82) as

$$\mathbf{x} = R(\cos\varphi, \sin\varphi, 0), \quad \mathbf{y} = R(1,0,0), \quad d\mathbf{l}(\mathbf{x}) = \mathbf{i}_\varphi R d\varphi = (-\sin\varphi, \cos\varphi, 0) R d\varphi, \tag{83}$$

where φ is the polar angle for the reference frame centered at the ring center. Substituting this into Eq. (82), we obtain

$$\begin{aligned} \mathbf{v}(\mathbf{y}) &= \frac{\Gamma}{4\pi R \cdot 2^{3/2}} \mathbf{i}_z \int_{\epsilon/2}^{2\pi-\epsilon/2} \frac{1}{(1-\cos\varphi)^{1/2}} d\varphi = \frac{\Gamma}{4\pi R} \mathbf{i}_z \int_{\epsilon/4}^{\pi/2} \frac{d\psi}{\sin\psi} \\ &= -\frac{\Gamma}{4\pi R} \mathbf{i}_z \ln\left|\tan\frac{\epsilon}{8}\right| = \frac{\Gamma}{4\pi R} \mathbf{i}_z \left[\ln\frac{8}{\epsilon} + O\left(\epsilon^2\right)\right]. \end{aligned} \tag{84}$$

If the size of the line element in the VFM is l, then $\epsilon R \approx 2l$ and the total number of elements is $N = 2\pi R/l$. Hence

$$V_\epsilon^{(self)} = \frac{\Gamma}{4\pi R}\left[\ln\frac{4R}{l} + O\left(\frac{l}{R}\right)^2\right] = \frac{\Gamma}{4\pi R}\left(\ln\frac{2N}{\pi} + O\left(\frac{1}{N^2}\right)\right). \tag{85}$$

We also can determine the "effective" radius of the core for a given discretization (compare Eqs (58) and (85)),

$$\delta \sim 2le^{-1/4} \approx 1.5576l, \quad \frac{\delta}{R} \sim \frac{4\pi e^{-1/4}}{N} \approx \frac{9.7867}{N}. \tag{86}$$